Peer-reviewed version available at *Catalysts* **2020**, *10*, 897; doi:10.3390/catal10080897

Review

Progress of MOF derived functional materials toward industrialization in solar cells and metal-air batteries

Mohamed Elhousseini Hilal,[a,b,c] Abdelkhalek Aboulouard,[d] Abdul Rehman Akbar,[a,b] Hussein A. Younus,[e,f] Nesrin Horzum,[g] and Francis Verpoort [a,b,h,i*]

a. State Key Laboratory of Advanced Technology for Materials Synthesis and Processing, Wuhan University of Technology, Wuhan 430070, China

b. School of Materials Science and Engineering, Wuhan University of Technology, Wuhan 430070, China

c. Chemistry and Environment Department, Faculty of Science and Technology, Sultan Moulay Sliman University, Beni Mellal 23000, Morocco

d. Laboratory of Sustainable Development, Sultan Moulay Sliman University, Beni Mellal 23000, Morocco

e. Department of Chemistry, Faculty of Science, Fayoum University, Fayoum 63514, Egypt

f. College of Materials Science and Engineering, Hunan University, Changsha 410082, China.

g. Engineering Sciences Department, Izmir Katip Çelebi University, 35620 Izmir, Turkey

h. Ghent University, Global Campus Songdo, 119 Songdomunhwa-Ro, Yeonsu-Gu, Incheon 406-840, South Korea.

i. National Research Tomsk Polytechnic University, Tomsk 634050, Russian Federation

E-mail: Francis Verpoort - francis.verpoort@ghent.ac.kr

Keywords: (Metal organic frameworks, catalysts, metal-air battery, solar cells, energy storage, energy)

Abstract

The cutting-edge photovoltaic cells are an indispensable part of the ongoing progress of earth-friendly plans for daily life energy consumption. However, the continuous electrical demand that extends to the night time requires a prior deployment of efficient real-time storage systems. In this regard, metal-air batteries have presented themselves as the most suitable candidates for solar energy storage, combining extra lightweight with higher power outputs and promises of longer life cycles. Scientific research over non-precious functional catalysts has always been the milestone and still contributing significantly to exploring new advanced materials and moderating the cost of both complementary technologies. Metal-organic frameworks (MOFs) derived functional materials have found their way to the application as storage and conversion materials, owing to their structural variety, porous advantages, as well as the tunability and high reactivity. In this review, we provide a detailed overview of the latest progress of MOF-based materials operating in metal-air batteries and photovoltaic cells.

1. Introduction

The 21st-century daily life environment is increasingly conjoined with robotics, information technologies, and artificial intelligence. The promise of a more simplified future of assigning numerous delicate tasks to intelligent machines and expecting inferior error rates has paved the way for further developing existing technologies as well as the emergence of others, ranging from 5G network to assisted electric vehicles and smart homes.[1][2][3] Several similar high-technologies have already been implemented and progressively claiming a significant share of the market. Therefore, the demand for electrical energy will only keep spiking henceforth, with a 2.1% growth per year of the global electricity demand, rising electricity share among other energy sources from 19% in 2018 to 24% in 2040.[4] Sourcing and storing this form of energy is nowhere around the optimum yet, even though conventional batteries and specifically the Lithium-ion (Li-ion) batteries have indeed revolutionized the history of storage devices and dominated the market of solar energy storage, due to their high energy density, relatively lightweight and the long operation life. But some recorded unfortunate incidents have pinned doubts worldwide on the Li-ion batteries.[5][6] In addition, the ever-increasing need for more powerful storage devices leads the research laboratories to expand their investigation and explore more reliable alternatives with higher energy densities.[7][8] Metal-air batteries (MAB) present a far more ecological and secure candidate with much higher energy density than the best lithium battery conceived to date, almost approaching gasoline [9], and potentially serving as the future solar energy storage devices.[8]

Both energy conversion and storage have always been complementary, coupling solar panels with MAB systems is a cutting edge technology used by pioneer energy companies.[10] The development of functional materials for both ends has been of cumulative progress. However, only a few operative materials have successfully made it out to the industrialization phase. Technically, for effective energy storage within MABs, oxygen evolution and reduction reactions (OER and ORR) are heavily involved, being the pivotal reactions, and at the same time, the bottleneck in the process, particularly with their high overpotentials. The industrially standard catalysts are always precious metals/metal oxides such as Pt, RuO_2, and IrO_2, by virtue of their excellent catalytic efficiency. Nevertheless, these rare, expensive materials are far from

being multifunctional, for instance, Pt has poor OER activity while RuO_2 and IrO_2 are not good options for ORR, besides bigger stability problems and low surface area. However, metal–organic frameworks (MOFs)-derived materials are currently the most eye-catching for research, with great potential to serve the industry. Thus, they are derived highly conductive and active sites-rich carbon materials have been among the most solicited materials for this issue.

MOFs are formed from a metal cation center and an organic ligand, coordinated with defined crystallinity and porosity.[11] Their high tunability and synthesis controllability acquire them with a wide range of characteristics and crystalline porous structures with BET surface areas up to 7800 m^2/g.[12] Due to their generally weak intrinsic conductivity and stability in harsh environments.[13] They are mostly used as precursors to produce numerous functional derivatives, inheriting well-developed porosity and porous carbonaceous structures, as well as chemical constituents and morphology, which would eventually evolve into well dispersed and accessible active sites, which intern lead to improved catalytic performance. MOFs have proven efficient not only for the storage but also for the conversion of light into electrical energy, combining two of the major potential solutions for nowadays energy crisis.[14]

MOFs-based materials have been widely studied in solar cell applications, due to their appealing physicochemical properties, great stability, large surface area, flexible structure, and low cost, serving as photoelectrode, counter electrode, and electrolyte for dye-sensitized solar cells (DSSCs).[15][16][17] MOFs have also been extensively used in perovskite solar cells (PSCs) to improve crystallinity, morphology, and absorption in the visible region of perovskite as well as photovoltaic performance.[18] However, organic solar cells (OSCs) based MOFs have not been extensively reported in the literature. The interesting results reported from the use of MOFs in PSCs and DSSCs would hopefully motivate the researchers to improve the efficiency of OSCs based MOFs. Herein, we have carefully selected and summarized the latest and milestones researches revealing recent progress of MOF-based materials, for both pivotal energy solutions.[19]

MOF based functional materials for solar cells

2.1.MOFs in dye-sensitized solar cells

Over the last few decades, many researchers have focused on dye-sensitized solar cells (DSSCs) due to their simple manufacturing and the ability to use inexpensive materials.[20][21] A standard DSSC is composed of: counter electrode, redox couple electrolyte, photoelectrode, as represented in **Figure 1a**.[22] TiO_2 has been commonly used as a semiconductor material that is frequently deposited on fluorine-doped tin oxide (FTO) as a thin film by using a doctor blade technique or screen printing. To enhance the cell's efficiency,, the photoelectrode must have some criteria such as wide surface area and good transparency.[23] In a typical DSSC, the dye is a ruthenium complex adsorbed on the TiO_2 surface and captivates sunlight photon.[24][25] During illumination, the dye gets excited from the ground state to the excited state and injects electrons into the conduction band of TiO_2. The dye became oxidized and the electron gets diffused to the counter electrode via the external circuit. For the counter electrode, platinum is extensively used thanks to inherent catalytic characteristics. Afterward, a liquid electrolyte, commonly consisting of redox iodide/triiodide (I^-/I_3^-), is used to regenerate electrons and relax the dye to its ground state.[26] Due to their good surface area, interlinked porosity, and structure flexibility, MOFs have been applied in DSSCs, which led to a noticeable improvement in cells' performance. MOFs application in DSSCs included its uses as a photoelectrode, counter electrode, and also as an electrolyte. The states of the art of MOFs-based DSSCs are discussed in the following sections.

2.1.1. MOFs for DSSC photoelectrode

A recent study was reported by He et al., where they utilized MOFs (ZIF-8 and UIO-66) and reduced graphene oxide (rGO) to modify the TiO_2 photoelectrode to enhance the photovoltaic performances of DSSCs.[27] In that composite, MOFs offer a high BET surface area for further dye adsorption, and rGO behaves as the collector of an electron to facilitate the transportation of electron from dye to the transparent conductive substrate. The short circuit density (J_{SC}) and conversion efficiency (η) of a simple TiO_2 photoelectrode are 11.6 $mAcm^{-2}$ and 4.55% respectively, however, by using a modified photoelectrode with MOFs and rGO, improved J_{SC} and η were observed reaching 17.8 $mAcm^{-2}$, 7.33% and 18.6 $mAcm^{-2}$, 7.67% for ZIF-8-RGO/TiO_2 and UIO-66-RGO/TiO_2, respectively. This enhancement is due to the increased dye adsorption on the photoelectrode.

ZIF-8 has also been reported as a blocking layer on the TiO_2 surface. Li et al. had demonstrated that the open-circuit voltage (V_{oc}) of DSSC could be improved when a thin layer of ZIF-8 (~ 2 nm) was deposited on TiO_2. This could be attributed to the inhibited recombination of interfacial charge as a result of the addition of ZIF-8 as a shell.[28] The same approach has been reported by using tris(2,2′-bipyridine) cobalt (II)/(III) redox as an electrolyte; the DSSCs show an improvement in J_{SC}=11.89mAcm^{-2}, V_{oc}= 881 mV, η= 7.75% to J_{SC}=14.39 mAcm^{-2}, V_{oc}= 897 mV, η= 9.42% (**Figure 1b**). This improvement is due to the enhanced electron lifetime and the amount of the dye adsorbed on TiO_2, as well as the absence of the TiO_2 conduction band shift once ZIF-8 treatment was applied.[29] However, ZIF-8 was not exclusively used as a blocking layer for the photoelectrode but also as a composite material. The TiO_2 aerogel–MOF nanocomposite has been utilized in the photoelectrode, but the conversion efficiency was 2.34%.[30] To achieve good efficiency, the density of the electron trapping sites and the insulation properties must be optimized by decreasing the MOF content in the composite material. [30]MOFs were also used as sensitizers and co-sensitizers because of their hierarchically organized structures and appealing light-harvesting properties.[15] A series of zirconium (IV) based MOF that integrate ruthenium (II) polypyridyl are grown as sensitizer on TiO_2. Nevertheless, the cells efficiencies are lower than 1%.[31]

2.1.2. MOFs for DSSC counter electrode

The counter electrode (CE) is an essential component of DSSCs which heavily affects the conversion efficiency of cells.[32][33] The CE has the role of collecting electrons from the external circuit and catalyzing the couple mediator in the electrolyte. The platinum is generally used as CE, as mentioned in the previous section. Due to its high cost, researchers have been utilizing alternative materials with low cost, good stability, and high catalytic characteristics.[34][35][36] Nowadays, MOFs were intensively studied for their appealing physicochemical properties which render them interesting materials for CE.[37][38][39] However, their employment as CE is quite limited due to the inherent mild conductivity, and the development of composite materials, including MOFs as well as conductive polymers, is typically needed to achieve the transport of charge in such application.[40]

Liu et al. have synthesized MoS_2@Co_3S_4 composites-based material as CE via the hydrothermal route using ZIF-67 as a precursor. The conversion efficiency of 7.86% was obtained which is higher than that obtained with Pt CE (6.99%). This improvement was rationalized based on the good specific surface area and catalytic properties (**Figure 1c**).[41] A transparent $CoS_{1.097}$@N-doped carbon film derived from cobalt−metalloporphyrin MOF thin film was prepared on FTO as CE for bifacial DSSCs. The latter showed higher conversion efficiency (9.11% and 6.64% respectively) from the front and back illumination than Pt (8.04% and 5.87%) and with extended long-term stability.[42] Similarly, a transparent CE for bifacial DSSCs was also developed using *van der Waals* layer-by-layer (lbl) epitaxial growth protocol for preparing porphyrin-based MOF *using* (5,10,15,20)- tetra (4 carboxyphenyl) porphyrin ligand and zinc acetate (call Zn- TCPP)39. The conversion efficiencies of front and rear sides were reported to be 5.48% and 4.88%. This outstanding performance was attributed to the presence of single Pt atoms in porphyrin struts and to the SURMOF thin film high transparency.[43] Another excellent composite CE was prepared from ZIF-8 and polystyrene sulfonate-doped poly (3, 4-ethylene dioxythiophene) ZIF-8/PEDOT: PSS. The conversion efficiency obtained was as high as 7.02% which is roughly equal to the yield of Pt CE (7.24%), making ZIF-8/PEDOT: PSS as a good choice to replace the expensive Pt.[17] Even higher efficiency of 8.91% could be obtained when a new zirconium-based MOF-525 and sulfonated-poly(thiophene-3-[2-(2-methoxy ethoxy)-ethoxy]-2,5-diyl) (s-PT) composite film was deposited on a flexible carbon cloth substrate.[16]

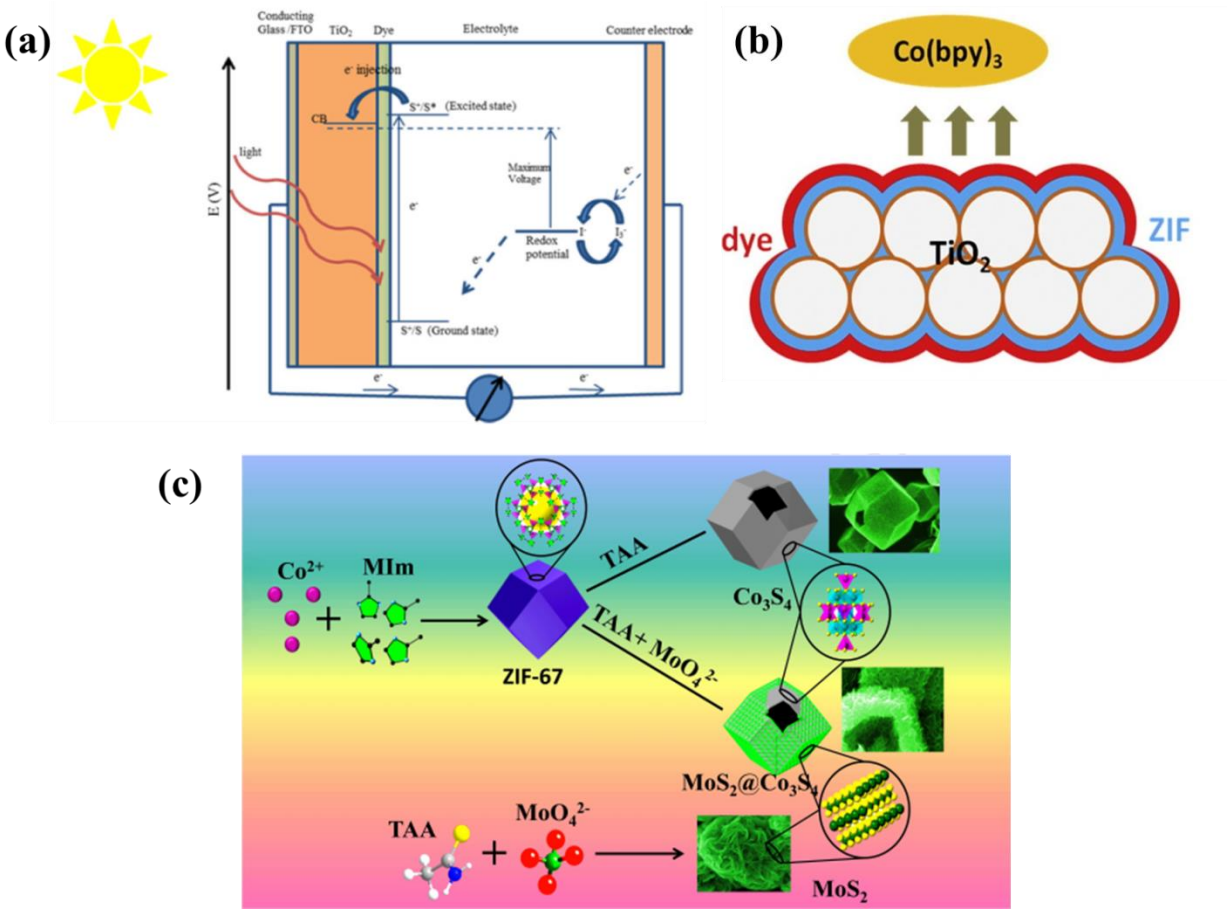

Figure 1: (a) A standard illustration of DSSC. [22] ***(b) ZIFs as electron blocking layers for TiO_2 photoelectrode with tris(2,2'-bipyridine) cobalt (II)/(III) as electrolyte.*** [29] ***(c)The preparation schema of $MoS_2@Co_3S_4$ composites-based MOF material ZIF-67.*** [41]

2.1.3. MOFs for DSSC electrolyte

The electrolyte is an essential component and widely investigated, as described in the previous section. However, the deployment of MOFs for electrolytes for DSSCs has been scarcely reported, for instance, Bella et al. prepared a polymer composite comprising a Mg-based MOF via UV-driven free-radical process. The conversion efficiency reached 4.8% with exceptional long-term stability.[44] Sarwar et al. mixed an Al^{3+} based MOF with a typical liquid electrolyte to form a gel electrolyte. The stability and photovoltaic performance of the gel electrolyte were significantly enhanced compared to liquid electrolyte alone.[45]

Preprints (www.preprints.org) | NOT PEER-REVIEWED | Posted: 17 July 2020 doi:10.20944/preprints202007.0364.v1

Peer-reviewed version available at Catalysts 2020, 10, 897; doi:10.3390/catal10080897

In conclusion, relevant studies have been done during previous years in order to use MOFs in DSSCs. The main issue that faced photoelectrode and counter electrode based on MOFs to the overpass was the relatively low electrical conductivity. However, MOFs application as electrolyte shows their long-term stability and good photovoltaic performance. MOFs proved with great potentials but still need to be studied with the objective to enhance the overall performance of DSSCs.

2.2. MOFs in perovskite solar cells

In recent years, perovskite solar cells (PSCs) have attracted the attention of researchers around the world due to their excellent photovoltaic performance. Continuous efforts have been paid to enhance the power conversion efficiency (PCE) throughout the last decades. From 2009 to 2019, the PCE was increased from 3.8% to 25.2%, which exceeded those obtained by traditional solar cells (CIGS and CdTe).[46][47] Perovskite absorber, electrodes, hole, and electron transport layers are generally the components of PSC. The three different standard architectures of PSCs are illustrated as seen in **Figure 2**. [48]

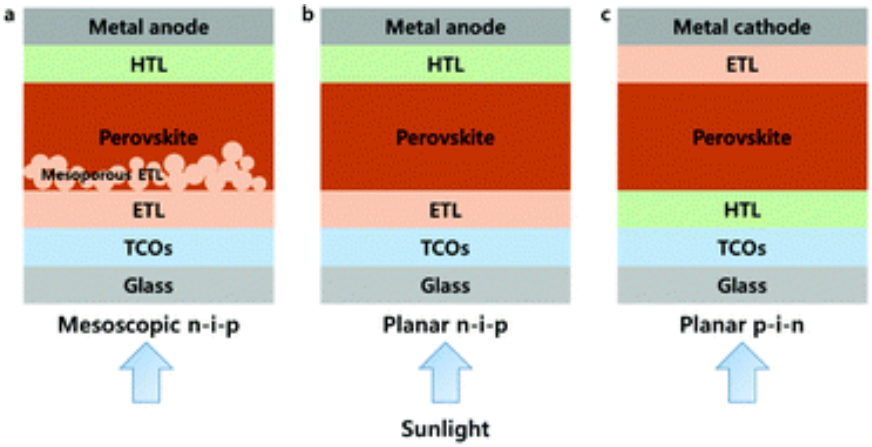

Figure 2: The standard architectures of PSCs: (a) mesoporous n-i-p, (b) planar n-i-p and (c) planar p-i-n. [48]

In order to enhance the performance of PSCs, MOFs have been extensively studied by virtue of its numerous physicochemical features.[49][50][51][52] MOFs have been used in PSCs in three ways:1- at the perovskite/ charge transporting layer (CTL) interface. 2- as the electron transporting layers (ETL) or hole transporting layers (HTL) or incorporated within CTL. 3-

within the interior of perovskite thin film. The recent progress of PSCs based MOFs is reported in the next section.

2.2.1. MOFs in the perovskite /CTL interface

Vinogradov et al. are among pioneers to introduce MOF in PSCs. TiO_2-MIL-125 was prepared to replace pristine TiO_2, which behaved as ETL, as shown in **Figure 3a.** Furthermore, the PSC shows long stability in the ambient atmosphere and the PCE reached 6.4%.[53] Moreover, porous hierarchical (hier-TiO_2) nanostructure was prepared by sintering the MIL-125(Ti) MOFs. The hier-TiO_2 is deposited on a compact TiO_2 layer, making a dispersed scaffold and consecutively making quasi-mesoscopic PSCs, which enables the growth of large and stable perovskite grains **(Figure 3b).** Consequently, the stability and photovoltaic performance (PCE= 16.65%) were higher compared to TiO_2 nanoparticles as a scaffold (PCE=11.38%) and TiO_2 compact based planar PSC (6.07%).[51] In the context of improving the sizes and the crystallinity of the perovskite as well as the photovoltaic performance, Shen et al. have incorporated ZIF-8 between mesoporous TiO_2 (mp-TiO_2) and perovskite interface serving as an additional scaffold to enable the development of crystals within perovskite. The optimum quantity of ZIF-8 would potentially crosslink adjacent perovskite grains, resulting in good growth of grains and satisfactory perovskite morphology, see **Figure 3c**. This incorporation proved effective for the elimination of carrier recombination and enhanced the extraction of charges. As a result, PCE of 16.99% could be attained which is superior to the cell with mp-TiO_2 **(Figure 3d)**.[18] A similar study where an inverted p–i–n PSCs were fabricated in order to enhance the efficiency of charge extraction and electrical contact between perovskite/NiO_x as an HTL interface by using two kinds of Zr-MOFs which are UiO-66 and MOF-808(**Figure 3e)**.The PCEs of modified PSCs are 16.55% and 17.01% for MOF-808 and UiO-66, respectively.[54]

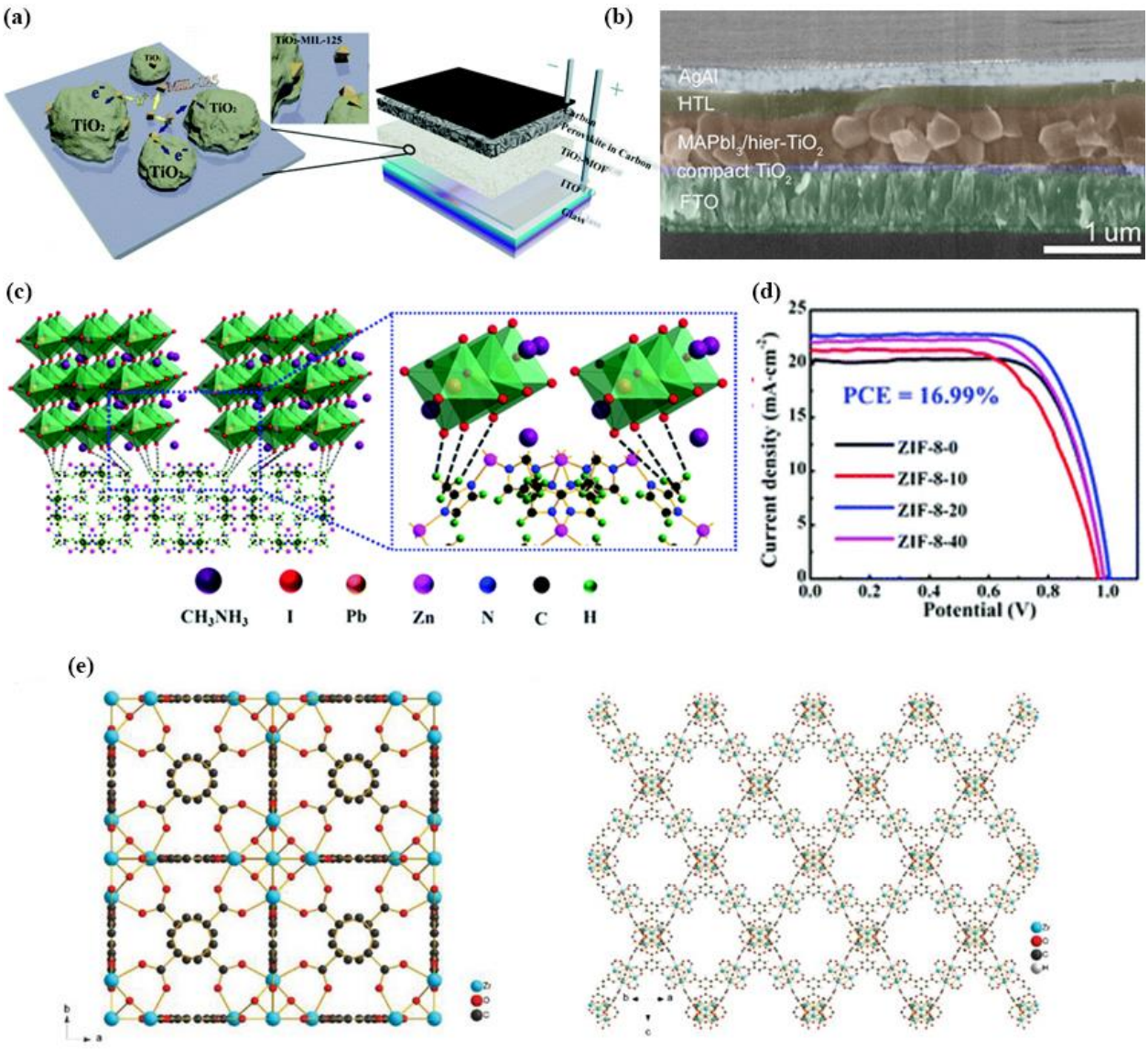

Figure 5: (a) Diagram structure of the photoactive composite and the depleted quasi-bulk heterojunction structure of TiO_2-MIL-125. [53] ***(b) Cross-sectional SEM of quasi-mesoscopic PSC using hier-TiO_2 deposited on compact TiO_2 layer.*** [51] ***(c) Schematic description of two adjacent grain structures linked by methyl groups of ZIF-8. (d) J-V curves of PSCs with ETLs containing ZIF-8-coated mp-TiO_2 for various times.*** [18] ***(e) The crystal structures of UiO-66 (left) and MOF-808 (right).*** [54]

2.2.2. MOFs for CTL or incorporated with CTL

By using MOFs as CTL or incorporated with CTL, the efficiency of charge extraction is significantly enhanced and the recombination of carriers is eliminated which improves the

photovoltaic performance. Nanocrystalline Ti-based MOF (MIL-125) have been synthesized in order to engender ETL and substitute the standard TiO_2 ETL. Furthermore, Ti-based MOF (MIL-125) was incorporated with PCBM ([6,6]-phenyl-C_{61}-butyric acid) to increase conductivity and inhibits the close contact of perovskite and ITO **(Figure 4a)**. Thereby, a good PCE was reached which is 18.94%.[55] By using the solvothermal method, Nguyen et al. prepared Co-doped TiO_2 with trimesic acid (H_3BTC) in the character of an organic framework to make the Co-doped Ti-MOF, see **Figure 4b**. The well-developed porous structure is obtained to use in PSC as an ETL. Therefore, an improved absorption in the visible region and a decrease in the hysteresis behavior has been observed, leading to an efficient charge extraction (PCE=15.75%).[56] Unprecedentedly, Yan and co-workers have employed ZnO instead of TiO_2 due to its higher electron mobility and structural heterogeneity which make it much more appealing. The as-synthesized ZIF-8-derived ZnO was used as ETL; this latter exhibits a particular morphology, great contact area, and large internal pores which leads to an intriguingly high PCE=18.1%.[57]

MOFs can also be used in HTL. Li et al. introduced a MOF, specifically, $[In_{0.5}K(3\text{-}qlc)Cl_{1.5}(H_2O)_{0.5}]_{2n}$, (In10) into (2,2′,7,7′-tetrakis(N,N′-di-p-methoxyphenylamine)-9,9′-spirobifluorene (Spiro-OMeTAD)) resulting in enhanced conductivity of HTL . As illustrated in **Figure 4c**, there is no large energy barrier between the In10 and Spiro-OMeTAD HOMOs. This leads to integrate In10 into Spiro-OMeTAD and could be advantageous for hole transfer at the perovskite-HTL interface, which in turn led to PCE of 17%. This achievement is attributed to the positive role of In10 in promoting perovskite sunlight absorption and avoiding penetration of moisture.[58] Huang et al. synthesized lead-based MOF $(Pb_2(1,3,5\text{-}HBTC)_2(H_2O)_4$, (Pb-MOF) which is doped into Spiro-OMeTAD material. In contrast to the simple Spiro-OMeTAD layer, the composite layer exhibits a smoother surface, great hydrophobicity, and electrical interfaces. The energy levels of Spiro-OMeTAD -MOF HTL in the PSC are more suit to the nearby layers of perovskite and Ag **(Figure 4d)**. Consequently, the PCE of the PSC based Spiro-OMeTAD -MOF HTL is 13.17% which is higher than that of the pure Spiro-OMeTAD HTL.[59] A planar heterojunction PSC was fabricated by Zhou et al. by implementing (MOF)-derived N-rich porous carbon (NPC) into HTL. This latter is composed of bidopants bis(trifluoromethane) sulfonimide lithium salt (Li-TFSI) and 4-tertbutylpyridine (t-BP) which are doped on Spiro-OMeTAD. This structure is achieved from the direct pyrolysis of a 2D In-based MOF In-Aipa, $[In_2(Hipa\text{-}NH_2)_2(ipa\text{-}NH_2)_2]\cdot 5H_2O$ ($H_2ipa\text{-}NH_2$=5-aminoisophthalic acid), as illustrated in **Figure 4e.** The

implementation of NPC decreases lithium salt aggregation and HTL defect formation, enhancing film quality for efficient hole extraction and redistribution. The fabricated cell has a PCE=18.51%.[60]

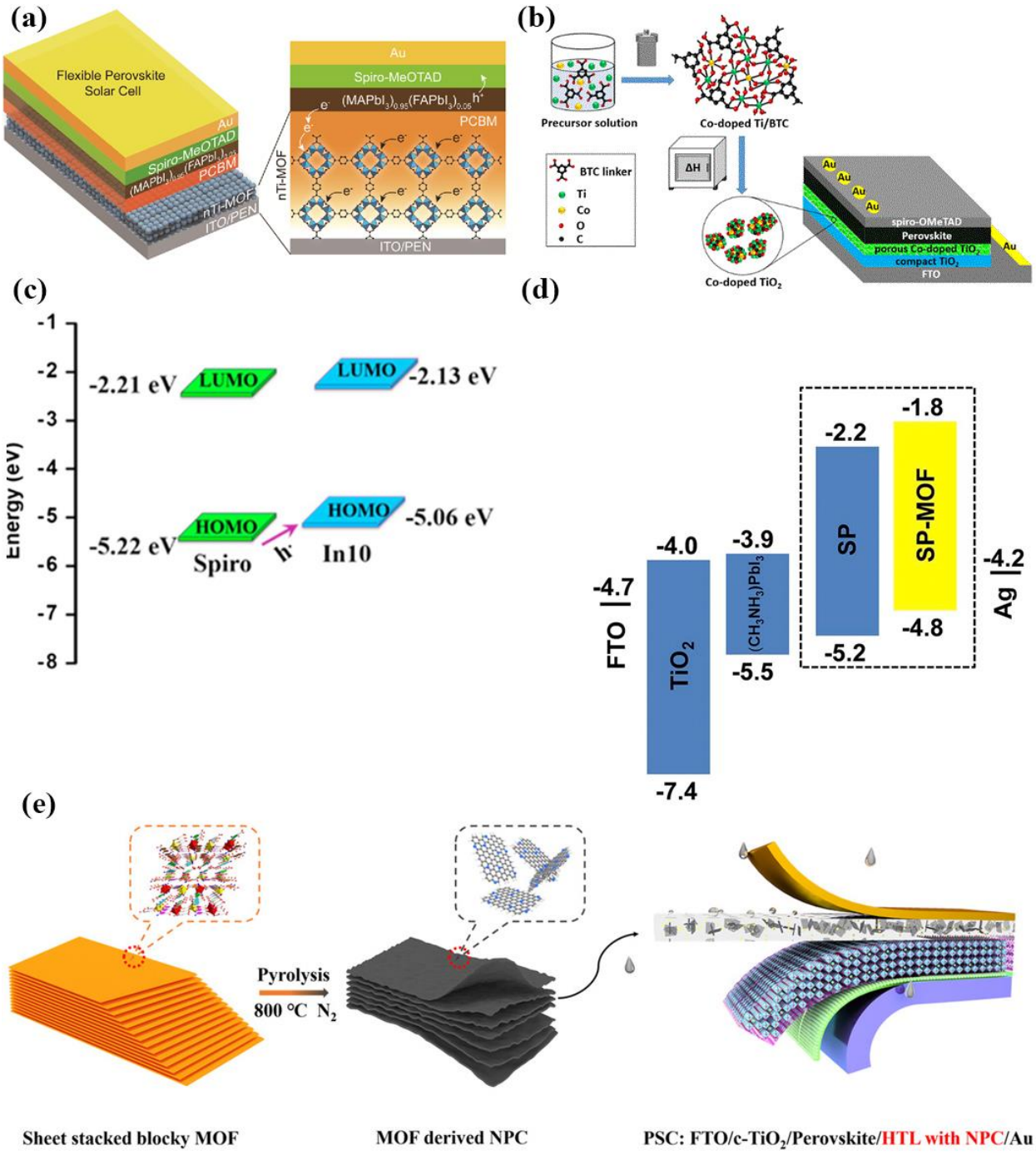

Figure 4: (a) Energy levels of Spiro-OMeTAD and In10, (b) J–V curves of HTM, and

HTM/In10 with different amounts of In10.[58] ***(c) The reflection spectra of Spiro-OMeTAD (SP) and SP-MOF samples, (d) Energy levels of PSC with Spiro-OMeTAD (SP) and SP-MOF as HTL.***[59] ***(e) The scheme of direct MOF crystals pyrolysis into graphitic NPC as HTL.***[60]

2.2.3. MOFs into perovskite thin film

The first study about introducing MOF into perovskite thin film was reported by Chang et al. A simple strategy to enhance the crystallinity of the perovskite thin film was achieved by introducing MOF-525 as additives in the precursor solution. This integration serves as a typical scaffold to permit perovskite to be crystallized inside. Therefore, the scaffold offers an orderly structure of perovskite crystallites during the initial crystallization stage. The PCE of the PCS with the enhanced morphology and crystallinity is 12%.[61] Lee et al. combined two types of Zr-based MOFs (UiO-66 and MOF-808) into the perovskite precursor. The resulting PSCs showed higher PCE= 18.01% and 17.81%, respectively. In addition, the long-term stability of PSCs based UiO-66 and MOF-808 are higher than the pristine cell.[54] Very recently, Zhou et al. have incorporated In(III)-based MOF, namely, [$In_{12}O(OH)_{16}(H_2O)_5(btc)_6]_n$ (In-BTC) with perovskite to form heterojunction light-harvesting layer to enhance light absorption, crystallinity, morphology, and stability of the perovskite thin film. The PCE of the resultant heterojunction perovskite/In-BTC is 19.63 ± 1.24%.[62]

In summary, MOFs have been used in PSCs to eliminate carrier recombination, enhance the efficiency of charge extraction, improve the absorption in the visible region, increase the long-term stability, and decrease the hysteresis behavior. Moreover, MOFs can enhance the morphology and crystallinity of perovskite thin film. Future works may open new roads to find other functions or advantages of MOFs in PSCs.

2.3. MOFs in organic solar cells

Organic solar cells (OSCs) are made from small molecules, polymers or both by easy and cost-effective techniques, like spin coating, printing and spray deposition. Thus, OSCs are inexpensive and simple to manufacture. The ITO is the most frequently used as transparent conducting oxide (TCO), obviously having a double function: the role of the anode in addition to allowing light to penetrate into the active layer. Then, PEDOT: PSS (poly(3,4-

ethylenedioxythiophene) polystyrene sulfonate) is deposited as an electron-blocking layer and it also enhances the movement of holes to the anode. In the bulk-heterojunction (BHJ) structure, the electron-blocking hole-transport layer (HTL) is important in contrast with the bilayer structure. The absence of HTL in BHJ results in low photovoltaic performance because the hole and electrons both move to the same electrode. Furthermore, the active layer contains organic materials which are acceptor and donor used as a layer to form bilayer cell or mixed to form BHJ cell. Carbon nanotubes (CNTs) have recently been utilized as accepters rather than organic acceptors to establish an active layer of the nanocomposite. The final component is the cathode that is mostly copper or aluminum (**Figure 5a**).[63]

As already discussed in the previous sections, the use of MOFs in DSSCs and PSCs has been well examined; however, MOFs application in OSCs have not been much investigated up to now. Xing et al. have recently succeeded in synthesizing a novel 2D tellurophene based MOFs by using cadmium nitrate and tellurophene-2,5-dicarboxylate. Afterward, polyethylenimine ethoxylate (PEIE) was utilized to exfoliate the 2D tellurophene based MOFs to make single- and multi-layer MOF nanosheets and used them as an electron extraction layer (EEL) for OSCs. When the hybrid MOF-PEIE was utilized as EEL it showed 15% improvement on photovoltaic performance compared to the PEIE layer thanks to the recombination of the suppressed charge and enhancement of the conductivity (**Figure 5b**).[19] This achievement opens new roads for MOF to be incorporated into OSCs.

Preprints (www.preprints.org) | NOT PEER-REVIEWED | Posted: 17 July 2020 doi:10.20944/preprints202007.0364.v1

Peer-reviewed version available at Catalysts 2020, 10, 897; doi:10.3390/catal10080897

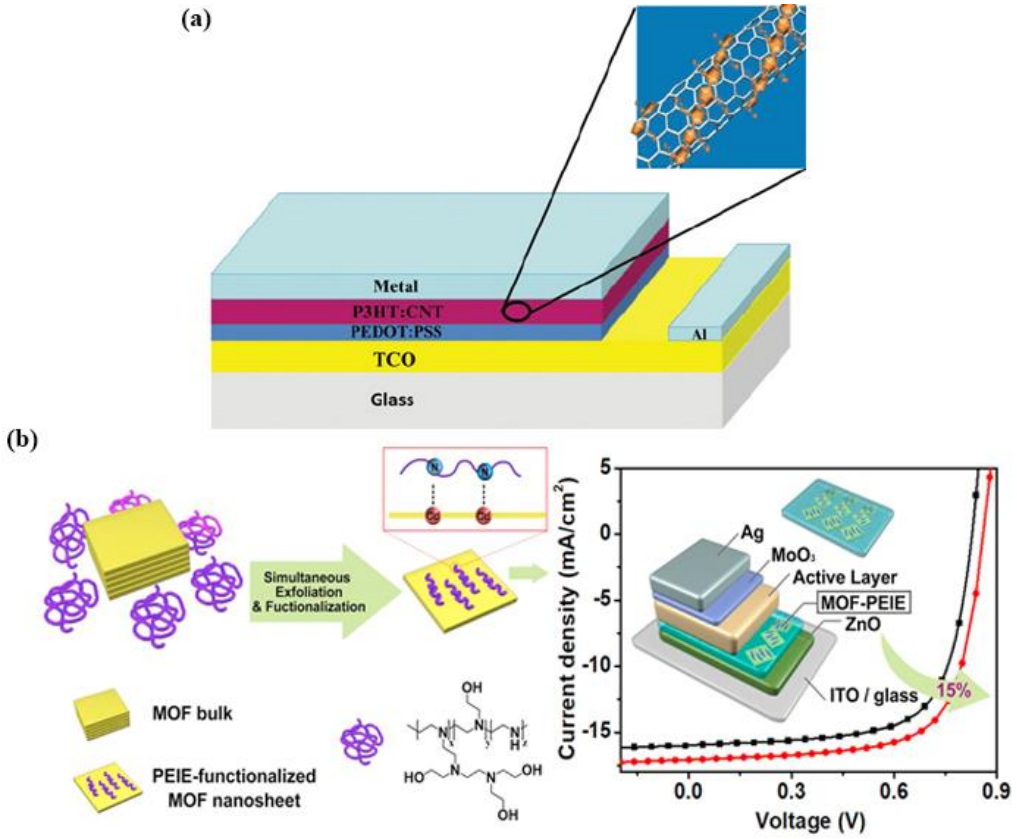

Figure 5: Diagram graphic of a standard organic basic cell using carbon nanotubes as an acceptor in the active layer. [63] ***(b) Preparation diagram of MOF-PEIE and its application in OSC.*** [19]

3. MOF based functional catalysts for metal-air batteries

Metal-air batteries (MAB) are generally composed of a metal anode, mostly Li, Zn, Al, Na … then a solid or liquid electrolyte and an air cathode, this applies on: (i) the mechanically rechargeable MAB, where the metal plate and sometimes also the electrolyte are changed after consumption during discharge. (ii) The solid-state MAB where the electrolyte is in the solid phase, generally PVA-based gel-polymer for Zn-air batteries. (iii) The electrically rechargeable MAB, that features an open battery model where the cathode is a breathing carbon-based or metallic porous foil, called Gas diffusion layer (GDL), supporting the indispensable bifunctional electrocatalyst. [64][65]

As a matter of fact, the performance of the MAB is systematically related to the quality of all three components. Nevertheless, the air-cathode electrocatalysts have attracted most of the attention, and that is due to hosting oxygen evolution and oxygen reduction reactions (OER and ORR), being the primordial reactions for the functioning of MAB. Therefore, the engineering of novel non-precious functional materials to accelerate the sluggish OER and ORR is of great importance. Over the past few years, MOFs stands out as a very promising and cost-effective candidate for air cathode materials, besides being a powerful tool to understand the functioning and the process during charging and discharging of the metal-air batteries, thanks to their tunability and design controllability.[66][67][68] MOF derived graphitized carbon facilitates the electrons transfers and proves strongly obstructing alteration during the charge-discharge process.[69][70][71] Besides that, the high surface area and the 3D porous structure not only multiply active sites and increase their accessibility but also favors the penetration of electrolyte and oxygen to successfully form the desired three-phase state.[72] Moreover, MOF-derived carbon materials could provide highly sought electrocatalytic bifunctionality, either by high dispersion of a single kind of catalytic active sites that could catalyze both reactions *i.e.* OER and ORR, or by containing bimetallic/heteroatoms based active sites or even host dual phases to approach the reactions in different mechanisms within the same catalyst.[73] This provides a profitable opportunity to synthesize and design a multitude of highly efficient bifunctional catalysts. Therefore, you will find hereafter the recently reported progress of MOF-based electrocatalysts specifically serving lithium-air batteries, zinc-air batteries, and others that are judged the most likely to be industrialized in the few coming years.

Zn-air batteries

The first Zn-air batteries have appeared in the early 19 century; however, their massive bulky nature with low current capacity didn't gain them much appliance.[74] In 1997, rechargeable Zn-air batteries returned to the surface by Miro Zorič.[74] Henceforth, many preliminary studies have been carried out to develop this technology as nowadays the most affordable storage option for an energy density reaching up to 1300 Wh.kg.[75] Extensive investigations on the anode materials and electrolytes have had a great impact on the industrialization of Zn-air batteries, overcoming the main challenges regarding dendrites, electrolytes leaks, and dryness. However, the bifunctional catalysts have been holding the most of the attention due to the key role of promoting vital reversible oxygen reactions. Actually, the discharge mechanism of rechargeable

Zn-air battery in aqueous alkaline media starts by the oxidation of Zn anode liberating couple electrons used for oxygen reduction reaction (ORR), the overpotential of this reaction is lowered by the electrocatalyst on the cathode; meanwhile, ZnO is formed by the reaction of the byproduct zincate ions to hydroxide and water.[76] During the charging process, the reversible process takes place and Zn cations get reduced and restore the Zn anode content.

- *Anode:*

$$Zn + OH^- \rightarrow ZnO + H_2O + 2e^-$$

- *Cathode: -*

$$½\ O_2 + H_2O + 2e^- \rightarrow 2OH^-$$

$$\text{Overall reaction: } Zn^{2+} + ½\ O_2 + \rightarrow ZnO\ (1.65V)$$

In laboratories, developing air-cathode bifunctional catalysts have taken serious steps forward recently using multiple technics and elemental combinations, but always, in order to reach a power density above 200mW/cm² and a high specific capacity over 800 mAh/g, coupled with significantly long life cycles, the bifunctional electrocatalyst should be carefully designed to be effective for both oxygen reactions and show excellent stability in such corrosive environment. Therefore, we will discuss hereby the most efficient and recent technics yielding state-of-the-art bifunctional catalysts for ZAB.

3.1.1. MOF-derived single-atom catalysts:

The single-atom catalysts have sparked important interest in their high electrocatalytic efficiency; this feature is directly inherited from the high atom utilization compared to other kinds of catalysts; The well-dispersed active metal atoms act very efficiently in hosting oxygen reactions for their high surface free energy.[77][78][79][80] Highly active FeN_4 sites have been anchored on 3D hierarchical carbon, derived from the pyrolysis of ferrocene-encapsulated ZIF-8 precursor. The resulting 3D hierarchically ordered microporous-mesoporous-macroporous

nitrogen-doped carbon 3DOM Fe-N-C-900 has successfully avoided common flaws of MOF derived Fe-C-N active sites being contained in microspores and often inactive (**Figure 6a**).[81] 3DOM Fe-N-C-900 has catalyzed ORR for ZAB and achieved a remarkably high power density of 235mW/cm² and a high specific capacity of 768.3 mAh/g_{zn}. The hierarchical carbon has exposed and stabilized single active atoms against migration by reducing their kinetic barrier of mass transport that usually causes agglomeration. The methanol tolerance test confirmed the high stability of the active sites with 90.2% retention after 20h continuous operation in contrast to 38.8% loss for Pt/C catalyst under the same conditions.[81]

Besides, iron and cobalt-based MOFs have always been attractive for ZAB air cathode catalysis, due to the fact that reduced Cobalt atoms get embedded in the N doped carbon matrix deriving from MOF at high temperatures.[82] The carbonization of heterostructured Co/Zn-ZIF@ZIF-67 has produced an interesting core-shell structure of single Co-N_xC_{4-x} active sites enveloped by highly graphitized porous carbon, as shown in **Figure 6b**. The number of N and C around Cobalt single atoms was tuned by pyrolysis temperature. At 900°C, Co-N_3C_1@GC single-atom catalyst is reported to dramatically enhance the mass transport and the electron transfer, which endorse the catalyst based ZAB, delivering a peak power density equal to 255 mW/cm² and outperforming Pt/C benchmark **(Figure 6c)**. It is to note that DFT calculations revealed that CoN_3C_1 is the best electrocatalyst, as compared to Co-N_2C_2 and Co-N_4, to exhibit near-Fermi electronic states, which promotes the electronic hybridization with O_2 and the step of protonation of adsorbed O_2*.[83]

Wagh et al. have designed single-atom coordinated hollow nano-spheroids of nitrogen-deficient carbon nitride by a two-step process, co-precipitation followed by annealing the metal-carbonitride complex to get supramolecular assemblies of metal single-atom catalysts. The absence of metal nanoparticle or clusters has confirmed the dispersion and confinement of single metal atoms by high magnification TEM. After testing the partially filled anti-bonding state of different metals (Cu, Fe, and Co), Cu turned out to be with the most suitable binding strength of intermediates with a d-band center value of -2.46 eV the closest to that of Pt (-2.67 eV), implying remarkable Oxygen reactions catalysis in **Figure 6d**. The intriguing exposure of Cu single atoms offered by the highly porous crumpled nano-spheroids has attributed CuSA@$HNCN_x$ based ZAB a high power density of 212 mW/cm² at 360 mA/cm², with a relatively high open-circuit voltage

(1.51 V) and specific capacity of 806 mAh/g_{zn} as shown in **Figure 7a**. The nitrogen stabilized Cu single-atom catalyst has proven stable cycling of over 1800 cycles (of 10 minutes each) @ 10 mA/cm^2.[84]

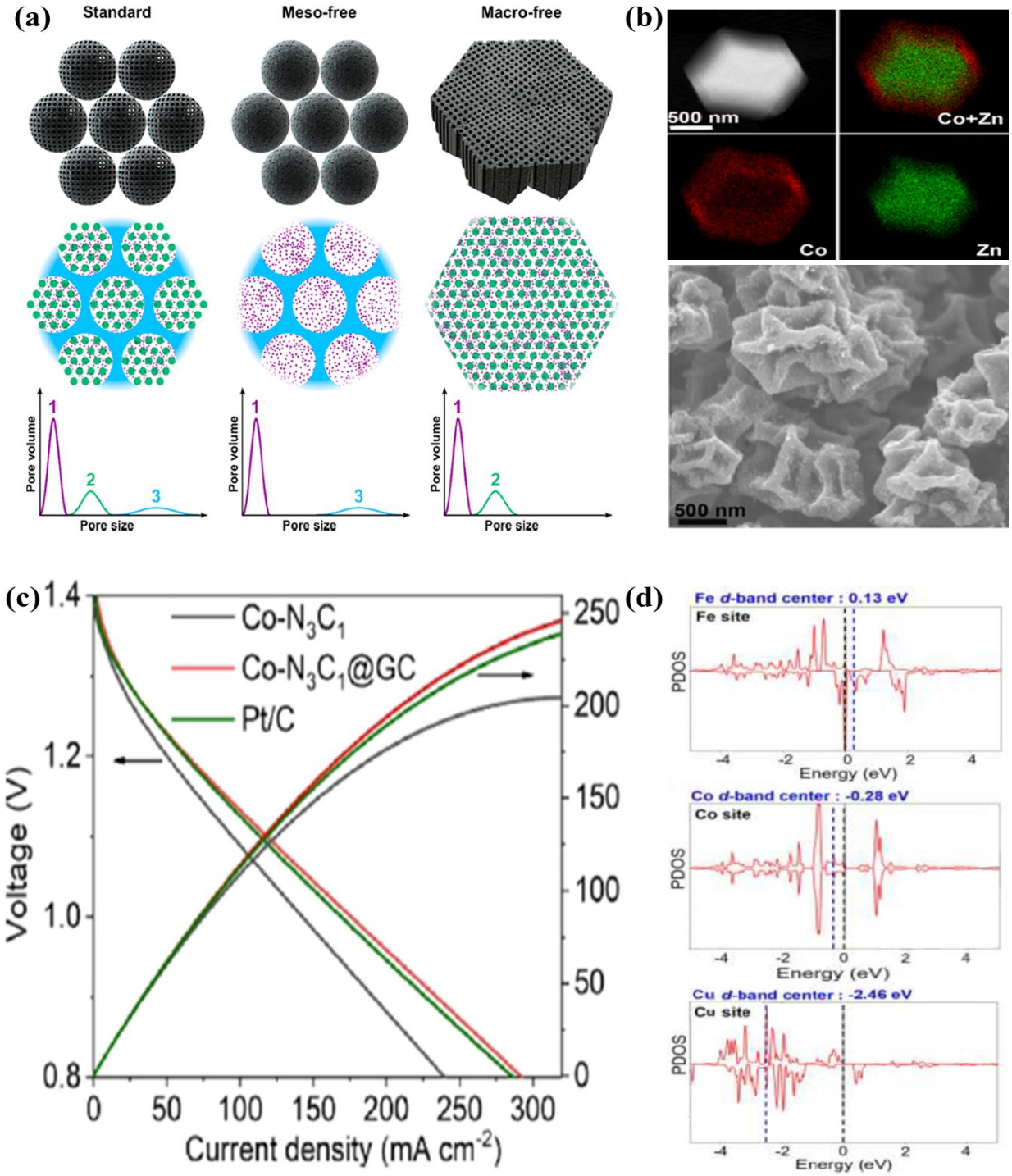

Figure 6: (a) The scheme and porous structures of the three model catalysts.[81] ***(b) The STEM-EDS elemental maps and SEM images of Co/Zn-ZIF@ZIF-67.***[83] ***The polarization curve and power density plot of the battery.***[83] ***(d) The partial density of states (PDOS) of Fe, Co and Cu in FeSA@HNCNx, CoSA@HNCNx, and CuSA@HNCNx, respectively.***[84]

3.1.2. MOF-derived bimetallic catalysts:

A successful synthesis of MOF-derived 3D carbon matrix composed of transition metal alloys has been a prominent way to acquire high-efficient and durable catalysts for ZAB's air cathode oxygen reactions. One very recent research has fabricated FeNi alloy nanoparticles inlaid by sacrificial ZIF-8 templating on nitrogen-doped carbon electrospun nanofibers. Tafel plots affirmed the important coupling of the bimetallic electrocatalyst by evaluating the slopes; FeNi/N-CPCF-950 has the smallest slope value of 67 mV/dec, whereas the rest of the samples with either iron or nickel-metal centers were much higher. Beside FeNi synergistic effects, the abundance of FeNi NPs in the hierarchically porous structures and the self-standing carbon structure thanks to the electrospun microfibers enabled FeNi/NCPCF-950 bifunctional catalyst to endow ZAB with a fairly high energy efficiency of 61.5%, with small charge-discharge voltage gap of 0.764 V, and more importantly, an outstanding 20 min charge/discharge cycles based astonishingly long stability performance of 640 hours at 10 mA/cm² under ambient conditions (**Figure 7b**).[85] In order to investigate the synergistic effect of multiple metal centers, two trimetallic catalysts for OER and ORR have been produced by Agarwal et al., starting from ZIF-8 supported on tellurium-derived porous carbon nanotubes and ZIF-67, and further doping Iron species. The resultant mixed-metals composites CoFeZn@pCNT (at porous carbon nanotubes) and CoNiFe-S@GC (at Graphitized carbon) derived from ZIF-67, were respectively used for ORR and OER of the ZAB air cathode. Showing a competitive round-trip overpotential of the cell is *ca.* 0.6 V.[86] Matériaux and co-workers have managed to synthesize a novel design of multiple transition metal bifunctional electrocatalysts Fe_2Ni_2N/Co@NCNT starting with the three metal cations Ni^{2+}, Fe^{2+}, and Co^{2+}. This design has developed highly dispersed trimetallic nanocrystals strongly coupled to a porous N-doped carbon, delivering an ultra-long life rechargeable ZAB exceeding 850 h at 5 mA/cm² with an outstanding 83 mV charge-discharge gap at 20 mA/cm².[87]

3.1.3. Heteroatoms doped MOF-derived carbon catalysts:

Recently, heteroatoms-doped carbon materials have attracted great attention by being environmentally benign and easily inserted into specific locations in the carbon matrix, and still exhibiting the ultrahigh active and atomically dispersion of metal atom – non-metal atom – carbon active sites, resulting in substantial decreases in ORR and OER overpotentials and efficient Zn-air battery performance.[88] The interest in this kind of doping stems from two mechanisms: the first whereby the high dispersion on the surface promotes the catalytic reaction, and the second where doped heteroatoms act as very reactive sites toward adsorption of water or hydroxide molecules to form oxygen gas.[86]

For instance, N-doped carbons have been the most investigated materials for Zn-air batteries, owing to inherent nitrogen electronegativity and the enhanced π bonding that improves electron-donor acceptor properties,[89] therefore electrocatalytic activity, high durability, and cost-effectiveness.[90] A recently reported dual-doped metal-free air cathode catalyst has shown impressive results open circuit potential of 1.48V, a power density of 208 mW/cm² and an energy density of over 870Wh/kg.[91] This P, N doped carbon has proven particularly promoting the adsorption of oxygen via the vacant 3d orbitals of P/N by valence electrons, as in **Figure 7c**.[92] P, N co-doping induced defects that led to highly localized states nearby Fermi level [93][94] improved the physicochemical properties of the carbon framework that boosted the electrocatalytic activity (**Figure 7c**).[95][96]

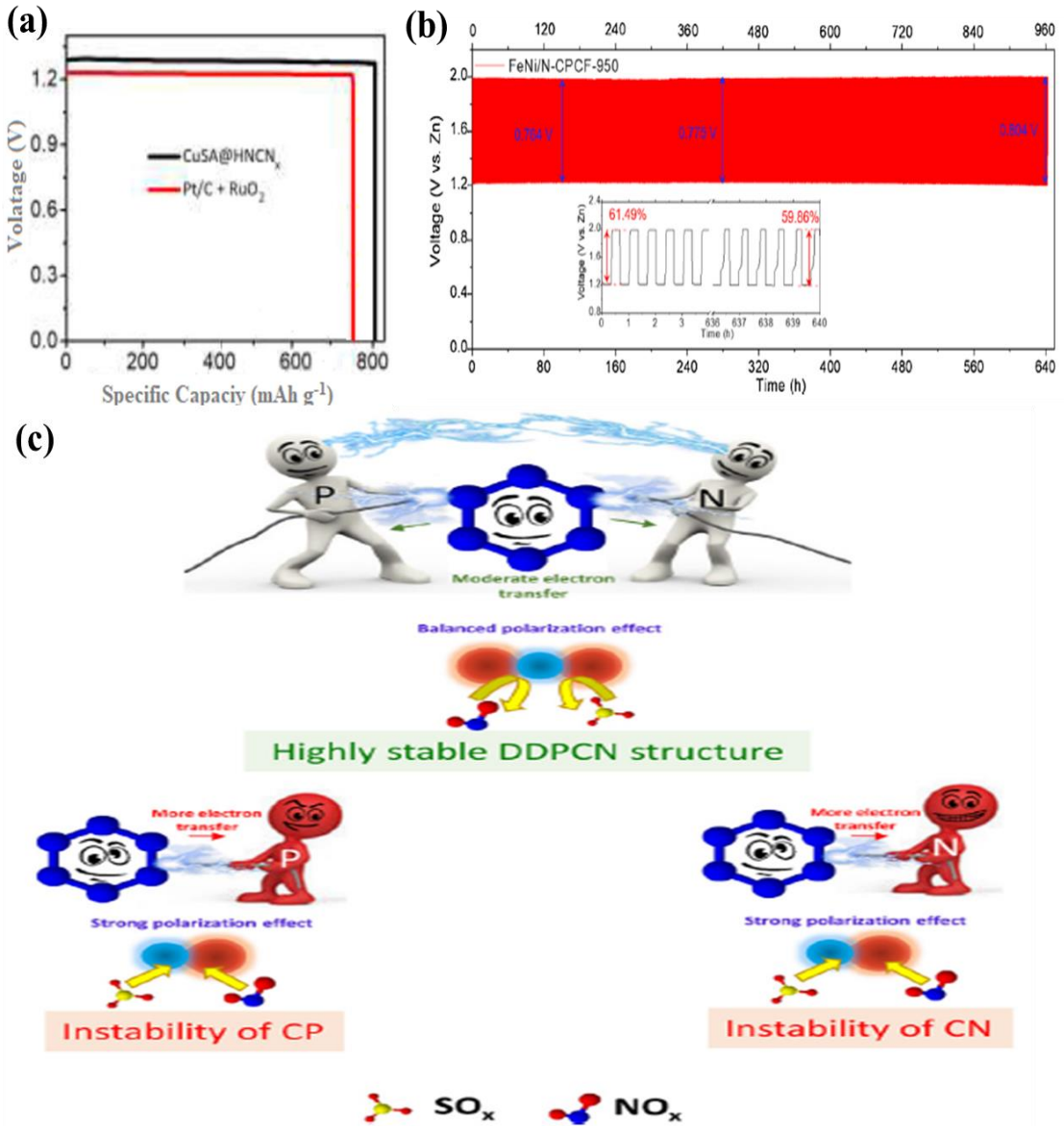

Figure 7: (a) Specific capacities of for CuSA@HNCNx and Pt/C+RuO₂ cathodes. [84] ***(b) The 640h galvanostatic cycling stability of Zn-air battery with FeNi/N-CPCF-950 air cathode catalyst (at 10 mA cm⁻²).***[85] ***(c) The structural resistance of P, N dual-doped porous carbon nanospheres (DDPCN), nitrogen-doped carbon (CN), and phosphorous-doped carbon (CP) for the incoming small molecules NO_x and So_x.***[91]

3.2. Li-air batteries

The lithium air/lithium–oxygen battery has wide-reaching consideration as the forthcoming energy source, owed to its very high theoretical energy density (~3500 Wh/kg).[97] Agraham et al.

have reported the first lithium-air battery with a structure of Li |organic electrolyte| air in 1996 followed by a series of work by other researchers.[98] Lithium-oxygen (Li-O_2) batteries got consideration as a prominent and efficient candidate in energy storage owing to their high potential energy densities and the plentiful and low-cost O_2 supply.[99] But for lithium-air battery, the discharge product Li_2O_2 is not soluble in an organic electrolyte and gradually chokes the porous air electrode.[100] Several technical encounters made it far behind the practical usage. The lethargic kinetic reactions at the air-electrode provoke serious issues, such as, the small round-trip efficiency and reduced rate capability. Though several efforts have been practiced to minimize the polarization, and certain progress has been accomplished, the cycle life is still relatively inadequate due to the deterioration of the electrolyte and anode.[97] Specifically, the huge overpotential needed for the Li_2O_2 recharge encouraged researchers to investigate effective Li_2O_2 charging catalysts. Bi-functional catalysts such as precious metals based (Pt-based, Ru-based) or metallic oxides (MnO_x, CrO_x, and CoO_x) revealed to be effective in decreasing the overpotential of the OER.[101]

The reaction mechanisms during discharge ORR and charge OER are the fundamentals for additional development while the overall electrochemical reaction of Li–O_2 batteries in non-aqueous is as follows in (Reaction 1):

$$O_2 + 2e^- + 2Li^+ \leftrightarrow Li_2O_2 \qquad \text{(Reaction 1)}$$

The discharge ORR mechanism in Li^+ containing non-aqueous solvents takes place in two major steps. The first step is the formation of superoxide (O^{2-}), which combines with Li^+ and surface-adsorbed $LiO_{2(ads)}$ and/or soluble $LiO_{2(sol)}$ in the solution are formed. The produced discharge intermediates experience another electron transfer on the surface of the electrode or a disproportionation reaction in the solution to form solid product, Li_2O_2, as shown in Reaction 2, 3, and 4.[102]

$$O_2 + Li^+ + e^- \rightarrow LiO_{2(ads\ or\ sol)} \qquad \text{(Reaction 2)}$$

$$LiO_{2(ads)} + Li^+ + e^- \rightarrow Li_2O_2 \qquad \text{(Reaction 3)}$$

$$LiO_{2(sol)} + LiO_{2(sol)} \rightarrow Li_2O_2 + O_2 \qquad \text{(Reaction 4)}$$

Peer-reviewed version available at Catalysts 2020, 10, 897; doi:10.3390/catal10080897

The reaction mechanism and intermediates (Li_2O_2) produced upon charging OER remain unclear. Peng et al. in their study excluded LiO_2 as the reaction intermediate during charging in acetonitrile, based on the absence of LiO_2 in the in situ surface-enhanced Raman spectroscopy (SERS) upon the charging process, instead, a direct two-electron process was proposed (Reaction 5).[102]

$$Li_2O_2 \rightarrow O_2 + 2Li^+ + 2\ e^- \quad \text{(Reaction 5)}$$

Another density functional theory proposed a superficial reaction way to produce off-stoichiometric based on topotactic delithiation of Li_2O_2 (Reaction 6, 7).[102]

$$Li_2O_2 \rightarrow Li_{2-x}O_2 + xLi+ + x\ e^- \quad \text{(Reaction 6)}$$

$$Li_{2-x}O_2 \rightarrow O_2 + (2-x)\ Li^+ + (2-x)\ e^- \quad \text{(Reaction 7)}$$

The experimental study utilized operando XRD showing that Li_2O_2 is oxidized through delithiation and form Li-deficient solid-solution (Li_2xO_2) phase in the tetraethylene glycol dimethyl ether solvent (Reaction 8, 9, and 10).[102] The main variance among Li_2O_2-oxidation mechanisms lies on the type of the major charging reaction intermediate species.

$$Li_2O_2 \rightarrow LiO_2 + Li^+ + e- \quad \text{(Reaction 8)}$$

$$LiO_2 \rightarrow O_2 + Li^+ + e- \quad \text{(Reaction 9)}$$

$$\text{and: } LiO_2 + LiO_2 \rightarrow Li_2O_2 + O_2 \quad \text{(Reaction 10)}$$

Among rechargeable batteries, Li–air batteries substituted the costly counterparts based on their compactness, low weight, and cost-effective because they espouse inexpensive and light oxygen during discharge. In Li–air batteries, air cathode prerequisite serious focus because of sluggish kinetics of ORR and OER, which is attributed to the low efficiency of catalysts. In order to get a drastically improved performance of lithium–air batteries an efficient catalyst needs to be integrated to attain lesser polarization. Therefore, to attain commercialized lithium–air batteries, the development of highly efficient catalysts for the ORR and the OER in air cathode should be a point of interest. The bifunctional catalysts could instantaneously enable the ORR and OER contributing to great progressions in the Li-air battery performance. The promising techniques to

develop MOF derived catalysts for Li-air batteries will be discussed in the upcoming section.[103][104]

3.2.1. MOF-derived metals/metal oxides/metal carbides based catalysts:

To develop effectively and established cathode catalysts to tackle the sluggish kinetics of the ORR/OER processes in Li-air batteries, MOF-derived metal oxides appeared as promising candidates.. Considering that performance evaluation for Li-O_2 battery occurs by electrochemical reactions occurring on the cathode, nanostructured advanced cathode materials designed for high energy densities have been developed. A novel and self-standing catalyst framework, where cobalt-based metal–organic framework (Co-MOF) was developed by 3D-printing to developed porous network geometry, was subjected to thermal annealing afterward. The exclusive framework provides effective deposition of Li_2O_2 particles during charging and then accelerates the decomposition of these insulating Li_2O_2 particles; this is attributed to the detention within well-controlled pores and the existence of Co-based electrocatalysts. The carbon framework itself possesses excellent conductivity and the required mechanical stability makes it a suitable conducting matrix. Consequently, the development of the porous matrix to self-standing catalyst construction can considerably raise the specific energy along with high energy density value up to 798 Wh kg^{-1}cell. Constructing 3D printed MOF derived framework cathodes provides an alternate new way to an enhanced practical, specific energy of the Li–O_2 batteries.[105]

An oxygen electrode was fabricated by stocking metal particles on the surface of porous carbon for Li−O_2 batteries. But nanoparticles are prone to lose contact during the reversible liquid−gas−solid reactions. To overcome such a problem, (Ru-MOF)-derived carbon composite electrocatalyst was prepared with stereoscopic Ru nanoparticles that are dispersed inside the carbon matrix. The high cycling stability is ensured based on the regeneration of the surface by Ru nanoparticles exposure performing as new active sites after the interacting surface Ru is lost due to detachment from the carbon oxidation during operation. Ru/carbon electrocatalyst construction prepared using Ru-MOF crystals as a precursor established stable charge−discharge cycling performance with 800 cycles for 107 days at normal room temperature and current

density of 500 mA/g and potentials 0.2/0.7 V (**Figure 8a**). It establishes a new window for the development of a better oxygen electrode of lithium-oxygen batteries (LOBs).[106]

MOFs as hybrid materials combining metal ions and organic ligands and having high porosity and vigorous structures have lately been anticipated as striking templates and precursors for manufacturing energy materials.[107][108] MOF- derived metal-nitrogen-carbon (M-N-C) catalysts gained massive attention because of high catalytic activity and low-cost for ORR & OER. Studies revealed that cathode catalysts with hierarchical porous structures significantly improve the performance of Li-O_2 batteries.[109][110] The metal-nitrogen (M-N_x) type efficiently provided active sites and enhanced the electric conductivity of the catalyst. However, a deficiency of balanced nanostructure production of the carbon catalyst makes the loaded metal nanoparticles cumulate during pyrolysis when the temperature is raised.

Hou et al. practiced vacancy engineering techniques to fabricate 2D micro-assembly Co_3O_4 nanosheets. The contents of oxygen and metal ions vacancy were adjusted by changing annealing temperature. It was found that the synergistic effects of the contents enhanced the electrochemical performance of the Li-O_2 battery. The study revealed that the highest number of defects led to premier electrochemical performance and displayed a discharge capacity of 8000 mAh/g along with electrochemical stability for more than 300 cycles under a specific capacity limit of 600 mAh/g at a current density of 100 mA/g. The concentration of oxygen vacancies in Co_3O_4 rises with increasing the annealing temperature from 200-400 °C, with the highest defects observed at 300 °C. The concentration of the structural defects controlled the electrocatalytic performances for Co_3O_4 since these defects provide rails for O_2 to pass into 2D micro-assembly Co_3O_4 nanosheets (**Figure 8b**) and it creates active sites that speed up ORR through the discharge procedure which facilitates to greater cycling stability. Electrocatalytic performances are also improved by ambient oxygen vacancies present in Co_3O_4 which assist mass transportation in speeding up the reaction between Li^+ and O_2 when ORR is happening and facilitates the deposition of Li_2O_2 films. This study opened new prospects to design transition-metal oxides as cathode materials for potential Li-O_2 batteries.[111]

In recent research work, the unique thermal and electrical conduction characteristics along with outstanding surface physicochemical features of the transition metal carbides (TMCs) made them the focus of attention.[112][113] Several carbides were utilized to enhance catalytic performance and activity, among them, molybdenum carbides were studied mostly by virtue of their high

electrical conduction properties and distinctive d-band electronic structures. Mo_2C and MoC got special interest as bifunctional catalysts in Li-O_2 for both ORR and OER reactions. The activity and permanence of Pt-based ORR electrocatalysts took a prominent enhancement by using MoC catalysts.[114] CNT as effective conductive materials for MoC_x, specifically heteroatom-doped CNTs doped with metals and nitrogen exhibited enhanced catalytic activity. N-doped CNT-encapsulated Co nanoparticles catalyst exhibited exceptional stability and excellent electrochemical activity in ORR. A bifunctional catalyst containing molybdenum carbide nanorods grafted with N-doped CNTs (NCNTs) was developed to stretch the electrochemical properties of Li–O_2 batteries. MoO_3 nanorods were coated with a Co-based ZIF-67 and treated to get MoC–Mo_2C/NCNTs nanocatalyst. The as-obtained nanorods have a distinctive structure that offers a large number of active sites and ample space for managing Li_2O_2 along with facilitating electrons transport via the catalytic active NCNT conductive paths. The synergetic effects of the three components Co, MoC, and NCNT considerably enhanced electrocatalytic performance of the composite catalyst in ORR and OER in Li–O_2 batteries. An extraordinary specific discharge capacity of 34862 mAh/g at current density 200 mA/g and cyclic stability of 162 cycles having a current density of 200 mA/g also considerably deprived discharge–charge overpotential. These results propose that the composite nanorod is an effective, steady bifunctional catalyst for potential Li–O_2 batteries.[115]

Preprints (www.preprints.org) | NOT PEER-REVIEWED | Posted: 17 July 2020 doi:10.20944/preprints202007.0364.v1

Peer-reviewed version available at Catalysts 2020, 10, 897; doi:10.3390/catal10080897

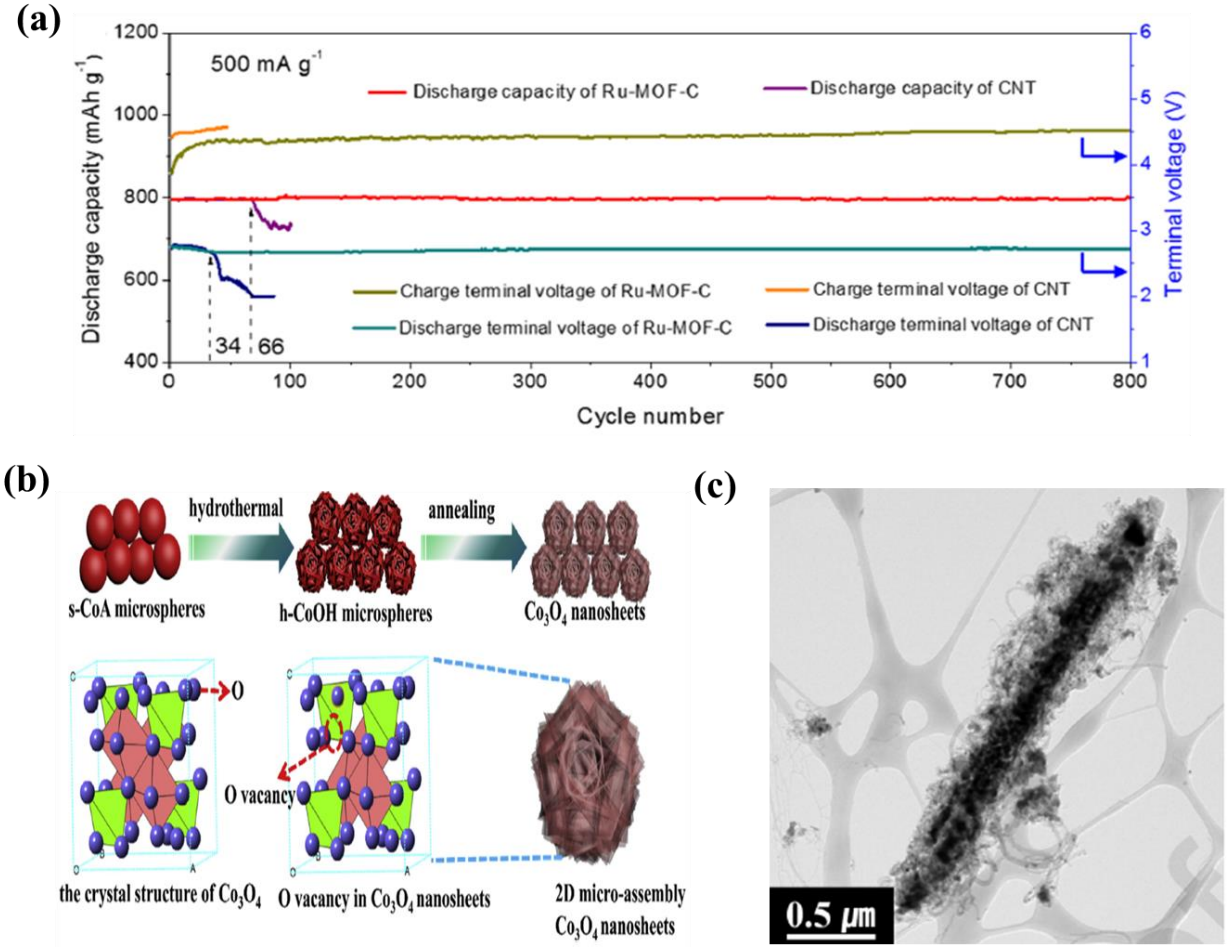

Figure 8: (a) The discharge capacities of the LOBs with Ru-MOF−C and CNT as the catalyst at a current density of 500 mA/g.[106] ***(b) The schematic representation of the synthetic procedure for 2D micro-assembly Co_3O_4 nanosheets.***[111] ***(c) MoC-Mo_2C/NCNTs nanorods TEM image at 0.5μm amplitude.***[115]

3.2.2. MOF-derived bimetallic and hybrid catalysts:

MOFs, its derivatives, and composites are enormously used as air electrodes and exhibited a greater discharge capacity attributed to its high specific surface area, distinct porous structure, and adequate active sites.[116][117] Recently, transition metal oxides/metal oxides appeared as a prominent constituent of Li–O_2 batteries air cathode. Co_3O_4 and $NiCo_2O_4$ based catalysts exhibited good ORR/OER activity and improved cathodic performance. The Li–O_2 batteries

based on single transition metal oxides suffer from poor specific capacity, insufficient cycling life, and small catalytic activity. Hence, a hybrid electrode with a synergistic effect between its components can increase the catalytic performance of the cathode. For instance, a bifunctional catalyst based nanoplatelets was synthesized with MnO_2- modified Co_3O_4 for Li–O_2 battery, where it displayed better electrochemical properties in comparison to the single component electrode.[103]

A hierarchical porous structure having microporous channels will enable fast O_2 diffusion. The mesopore structure can efficiently increase the electrolyte immersion whereas the macroporous one enables the kinetic availability of the active sites and accumulates additional discharge products. Nevertheless, most air-electrodes mentioned with macropores are metal oxides, and a very small proportion of bimetal-nitrogen-carbon (BM-N-C) materials derived from micro–meso-macroporous MOFs applied as the cathode of Li-O_2 batteries. However, a bifunctional catalyst, micro–meso-macroporous FeCo-N-C-X derived from hierarchical M-FeCo-ZIFs-X was synthesized (**Figure 9a**). Polystyrene microspheres templates were used, hierarchical M-FeCo-ZIFs-X worked as precursors, and after etching the templates M-FeCo-ZIFs-X nanoparticles with evenly distributed macropores were attained. M-FeCo- N-C-0.2 based cathode showed a high initial capacity of 18750 mAh/g at a current density of 0.1 A/g and exhibited good rate capability of 7900 mAh/g at a current density of 0.5 A/g after 192 cycles of stable performance. The exceptional performance accredited to the synergistic effect of Fe, Co nanoparticles, and N co-doping carbon frameworks having distinct micro–meso-macroporous structure.[118]

Another free-standing array structured Co_3O_4@$NiCo_2O_4$ cathode prepared by *in situ* growth of cobalt-based metal-organic framework (Co-MOF) sheets on carbon cloth (CC) and impregnation in nickel nitrate solution followed by pyrolysis under air-flow. The free-standing and binder-free Co_3O_4@$NiCo_2O_4$/CC cathode displayed extraordinary ORR/OER activity and greater cycling stability, a specific capacity of 10645 mAh/g (**Figure 9b**), and stability of 225 cycles without obvious degradation were achieved. [119] With the same vision, in Li-O_2 batteries, metal/metal oxide composite catalyst (Fe_2O_3@C@MnO_2) which combine Fe_2O_3 and MnO_2 displayed enhanced cycling performance and reduced charge voltage than single C and Fe_2O_3@C electrodes.[120]

Zhang and et al. designed and synthesized the metal hybrid catalyst Mn-MOF-74@CNTs as a cathode material for Li–O_2 batteries where Mn-MOF-74 nanoparticles were grown directly on carbon nanotubes using additive-mediated synthesis method. The formation of less-reactive discharge product LiOH compared to Li_2O_2 by the nano-architectured Mn-MOF-74@CNTs hybrid catalyst, Mn-MOF-74@CNTs-based oxygen cathode display fewer side reactions. The formed cathode displayed improved cycling performance even in a humid oxygen atmosphere where Li_2O_2 was made as discharge products.[121]

Dual metal–organic frameworks mixture containing MIL-100(Fe) and ZIF-8, was thermally activated in N_2 and then in NH_3 (**Figure 9c**). The subsequent catalysts demonstrated stacked carbon nanosheets (CNSs) morphology with a minor portion of carbon nanotubes (CNTs) protruding from the surface. The carbon matrixes were doped evenly with Fe and N species, and the present additional Fe generates Fe–Fe_3C particles to improve oxygen affinity and indorse *OH desorption. The formed catalyst exhibits outstanding ORR catalytic performance in alkaline/acidic half-cells, along with a PEMFC and also an aprotic Li–O_2 battery. The exceptional ORR catalytic presentation attributed to Fe–Fe_3C@Fe–N–C dual active sites, hierarchical porosities (micro/macropores) for bulk transport, and partial carbon graphitization for rapid charge transfer. These outcomes establish MOFs as model systems for the rational design of electrocatalyst for energy-based functional applications.[122]

One-step carbonization was used to synthesize core@shell-structured, hierarchically porous manganese oxide/cobalt manganite@nitrogen doped carbon (MnO/$CoMn_2O_4$@N–C) nanorods with interstitially decorated $CoMn_2O_4$ nanoparticles. MOF-coated with α-manganese oxide (α-MnO_2@ZIF-67) nanorods cathodes were used for LOBs to enhance the bifunctionality, cyclability of α-MnO_2 nanorod cathode-based LOBs along with specific discharge capacity. MnO/$CoMn_2O_4$@N–C nanorod cathode-based LOB shows a higher full specific discharge capacity of 8625 mAh/g and cyclability of 48 discharge–charge cycles at 200 mA/g specific current and 2000 mAh/g limited specific discharge capacity compared to their α-MnO_2 nanorod equivalents. Alike MOF-derived nanoparticle-decorated nano-constructions lead to high-performance tunable bifunctional electrocatalysts.[123]

Inquest to produce efficient and stable catalysts, composites made of carbon with embedded

metal/metal oxides fascinated great attention as electrochemical catalysts. However, intensive carbon evaporation during the pyrolysis synthesis causes reduced dispersion of the active sites and lower catalytic stability, to tackle the particles aggregation engendered an oxide shell was coated on precursor under high temperature. Liang et al. used Zn, Co zeolite imidazole skeleton coated by mesoporous silica functioned as precursor followed by pyrolyzation and Co, NeCNF catalyst was synthesized. Bimetallic Co, NeCNF catalyst has heteroatoms that demonstrate synergistic effects with other functional components that significantly enhance catalytic activity. The outstanding electrochemical performance with a high specific capacity of 5288 mAh/g along with outstanding cycle stability without substantial voltage reduction after 500 cycles was attained. The exclusive core-shell structure and metallic cobalt active sites contribute to excellent electrochemical properties.[124]

3.2.3. Non-metallic MOF-derived carbon dopants:

Noble metal and metal oxides, and hybrid showed excellent catalytic activities but their practical applications got limitation owing to their high cost. Developing proficient electrocatalysts with efficient structure is expected to be achieved to reduce the problems related to Li_2O_2 discharge products during the ORR/OER in Li-O_2 batteries. It will not only overcome the deprived rate capability but also increase the electrochemical properties of the LOB. Yu et al. reported the synthesis of cobalt nanoparticle *in-situ* encapsulated into nitrogen-doped carbon polyhedral under an Ar atmosphere, where ZIF-67 pyrolysis was conducted at a temperature between 700-1000 °C and optimal temperature of 900 °C was found. The as-prepared Co@NC and Co@NC-900/acetylene black material was implemented as bifunctional electrocatalysts and used as an oxygen electrode in Li–O_2 batteries. The cathode displayed discharge abilities of 3110 mAh/g and stable cycle life for more than 80 cycles along with the limiting capacities of 1000 mAh/g. The Co@NC-900/ AB electrode could be attributed as potential metal-based cathode electrocatalysts because of its electrical conductivity, suitable N content, large surface area and numerous active sites in Li–O_2 batteries.[125]

Thi et al. have reported a dual-phase carbon nanostructure for lithium–oxygen battery cathodes, by interlaced linkage of MOF-derived carbon and conductive carbon nanotubes. Carbonized MOF transforms into high porous carbon the formation of an effective and high capacity cathode.

Preprints (www.preprints.org) | NOT PEER-REVIEWED | Posted: 17 July 2020 doi:10.20944/preprints202007.0364.v1

Peer-reviewed version available at Catalysts 2020, 10, 897; doi:10.3390/catal10080897

Dual-phasic carbon nanostructure was constructed by growing MOF nanoparticles on the CNTs followed by the carbonization of MOF/CNTs. The formed structure includes the benefits of both components, MOF-C offers a large surface area, while CNTs deliver superficial pathways. Dual-Phasic Carbon Cathode exhibited that the synergistic nanoarchitecture of material demonstrated a high discharge capacity of 10050 mAh/g along with stable cycling performance over 75 cycles showing excellent electrochemical performance of LOBs.[118]

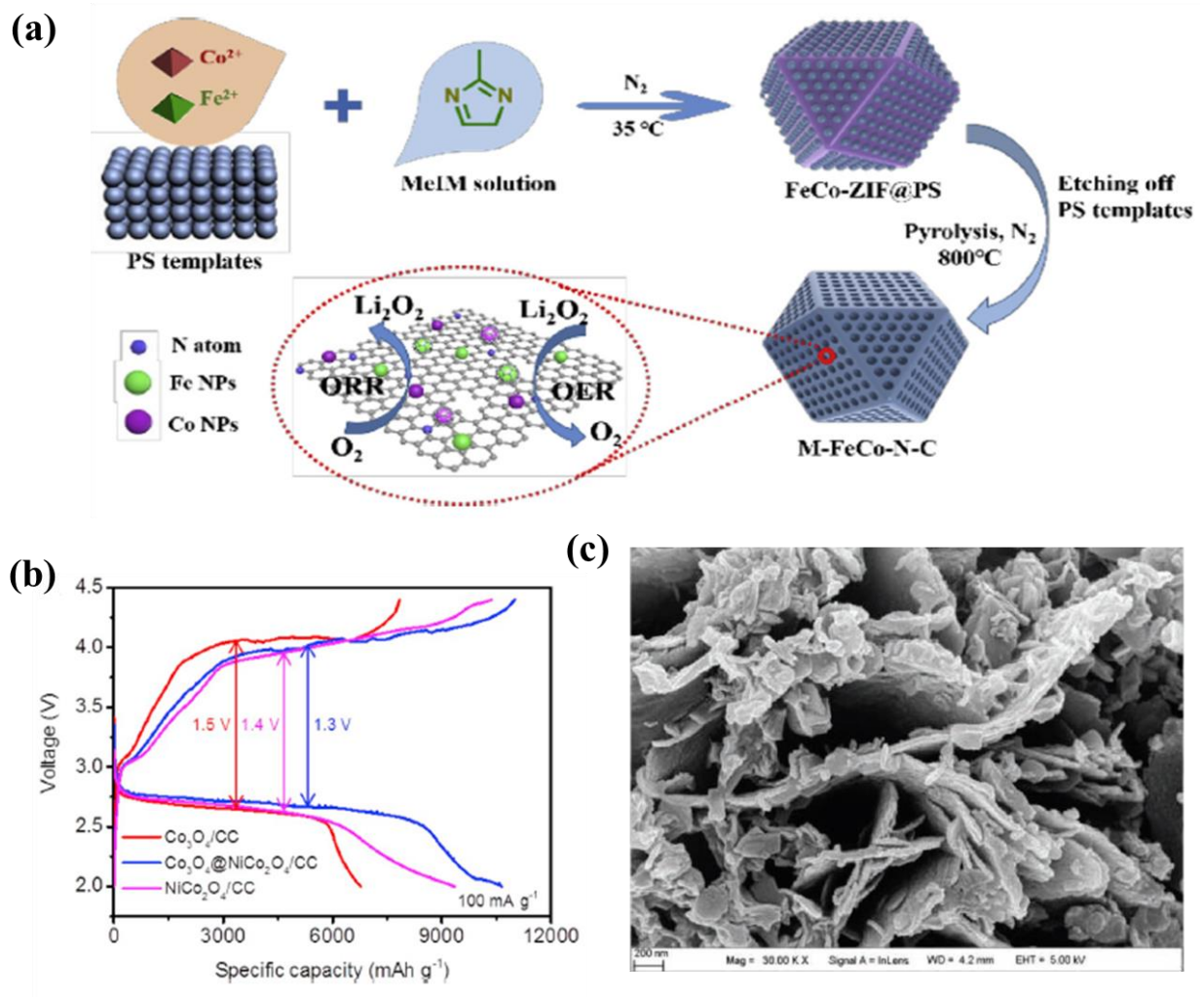

Figure 8: (a) The illustration of the synthetic process of M-FeCo-N-C-X catalysts.[118] ***(b) The first discharge–charge curves of Co_3O_4/CC, Co_3O_4@$NiCo_2O_4$/CC, and $NiCo_2O_5$/CC catalysts.***[119] ***(c) The FESEM image of 1MIL/40ZIF-1000.***[122]

Preprints (www.preprints.org) | NOT PEER-REVIEWED | Posted: 17 July 2020 doi:10.20944/preprints202007.0364.v1

Peer-reviewed version available at Catalysts 2020, 10, 897; doi:10.3390/catal10080897

3.3. Al-air batteries

Other active metals have been utilized as anodes for air batteries including Ca, Mg, Al, and Fe.[126][127][128] Aluminum (Al), a popular existing anode material for metal fuel cells and air batteries application, has a great advantage over other metals like its abundance, reasonable price, non-toxic nature, environment friendliness and recyclability making Al a promising candidate for next-generation energy storage equipment.[129][130] Al appeared as ideal material based on properties; it acquired like its trivalence and low atomic weight of 26.98g /mol, Al only lags behind Li in its theoretical specific capacity value that is 2.89 A.h/g. Moreover, by a value of 8.04 A.h.cm^3, the theoretical specific volumetric capacity of Al is the uppermost amongst the metallic fuels making it special.[131][130] The first Al-air battery was developed in the 1960's by Zaromb and it emerged as an efficient source with several applications.[132] Using Al-air as electric vehicle power by Alcoa and Phinergy company made it prominent in 2014. Nevertheless, the commercialization of Al-air batteries is still in development stages due to the high corrosion rate of Al anode in alkaline electrolytes and the polarization factor in neutral electrolytes because of insoluble oxide film formed on Al anode.[133][134]

A characteristic Al-air battery is generally composed of three components, an Al anode, an air cathode and an alkaline or brine electrolyte. The half-cell reactions on both electrodes are shown in (Reaction 11, 12), whereas overall Al-air battery reactions can be summarized as shown in (Reaction 13). The parasitic hydrogen evolution effect at the Al anode is shown in (Reaction 14).[135][136]

- *Anode:*

$$Al + 4OH^- \rightarrow Al(OH)_4^- + 3\ e^- \qquad (-2.35V) \qquad (11)$$

- *Cathode:*

$$O_2 + 2H_2O + 4e^- \rightarrow 4OH^- \qquad (0.40V) \qquad (12)$$

$$\text{Overall reaction: } 4\ Al + 3\ O_2 + 6\ H_2O + 4\ OH^- \rightarrow 4\ Al(OH)_4^- \qquad (2.75V) \tag{13}$$

$$\text{Parasitic reaction: } 2\ Al + 6\ H_2O + 2\ OH^- \rightarrow 2\ Al(OH)_4^- + 3\ H_2 \tag{14}$$

3.3.1. MOF-based electrocatalysts for Al-air battery:

The sluggish kinetics of cathodic ORR limits the power density of Al-air batteries. Electrocatalysts are vital for oxygen reduction reaction owing to involvements of multiple adsorption/desorption reactions where ORR undertakes in the "four-electron" pathway and produces extraordinary current efficiency and discharge voltage. To effectively increase active sites and speed up mass transfer, one could deploy metal content in a porous carbon matrix. The matrix restricts aggregation of metals to enhance ORR performance by more exposure of active sites to the interface. MOFs are considered as the favorite precursors to prepare carbon matrix.[137][138][139] Silica stabilizing technique was used to develop a stable and efficient electrocatalyst where CoNi bimetal nanoalloy uniformly embedded in N doped carbon framework for Al-air batteries. The etching process followed by silica stabilization generates pores in the produced CoNi-NCF (Nitrogen-doped carbon framework) electrocatalyst. A large number of active sites in CoNi nanoalloy, porous structure, high specific surface area, and stable conductive carbon matrix made the CoNi-NCF exhibit excellent ORR performance. A half-wave potential of 0.91 V was achieved in 0.1 M KOH solution and 0.64 V in 3.5 wt% NaCl solution. When CoNi-NCF was employed as a cathode catalyst in aqueous and solid flexible Al-air batteries, active sites improved the ORR performance and highest discharge performance, and longtime durability and high flexibility were achieved.[140]

Liu et al. developed bimetallic spinel-type hollow nanocages ($ZnO/ZnCo_2O_4/C$) derived from the ZIF-67/GO/$Zn(NO_3)_2$ precursors. The ZIF-67 helped in obtaining a hollow cage structure with more active sites and a higher surface area. The active sites and surface area were further enhanced by the dispersion of MOF particles on reduced GO. The presence of rGO in the hybrid structure enhances the overall electrical conductivity and leads to a better performance in the battery.[141] Cu-centered MOF precursor was used to modifying the Ketjenblack (KB) carbon to

make a novel hybrid catalyst. The synergistic effect between crystalline Cu/Cu_2O nanoparticles and noncrystalline CuN_xC_y species, produced by the calcination, enhanced the catalytic activity of the modified KB carbon toward ORR. The excellent performance of the as-manufactured hybrid catalyst was exhibited, where half-wave potential and larger limiting-current density was shown compared to 20 %wt Pt/C. A high stable voltage of 1.53 V at a working current density of 40 mA/cm^2 was marked on the home-made Al–air batteries.[142]

A simple double-phase encapsulation and post heat treatment method was used to structure a hierarchical porous N, S-co-doped carbon where cobalt-nickel-sulphide nanoparticles are encapsulated inside. Integrated hybrid architecture Ni-Co-S@G/NSC displayed an onset potential of 0.94 V, a greater discharge voltage plateau, enhanced stability, and half-wave potential to the commercial Pt/C catalyst in ORR and the full battery test. Superior ORR activity of the Ni-Co-S@G/NSC catalyst credited to greater surface area and pore volume and synergetic effect of the components. MOFs with a double-phase encapsulation approach contribute to design improved catalysts for Al-air batteries.[143]

3.4. Na-air battery:

Among hereby reported Metal-air batteries, Na exhibit relatively high theoretical values for specific energy where lithium-air batteries are catching up with the theoretical specific energy of gasoline. Factors like ingestion of solvent in the discharging process, blockage of pores, and the air cathode degradation and degradation of the air cathode limit the commercial success of Li-air batteries.[144][145] Na metal-based batteries appeared as a prospective substitute to lithium-based batteries due to its alike electrochemical features.[146][147] Sodium appeared as the most emerging replacement for lithium to meet the requirement of energy storage owing to its abundance in earth crust as the forth plentiful element sharing approximately 2.6% sodium by weight, as well as the easy availability and low cost. [148][149]

The reduction potential of 230 mV of sodium makes it store more energy owing to the fact that cells can produce large potential. Moreover, low atomic weight and higher electronegativity enable delivering high specific capacity. Combining metallic sodium with oxygen as an opponent reactant at the cathode provides the basis for Na-air batteries. The Na–air battery is counted as an environment-friendly electrochemical power storage device with developed energy density.[150] The value 1600Wh kg^{-1} of specific capacity in Na-air batteries is not as high as that of Li-air batteries but it is suitable for several devices in this range of capacity. The Na–air battery is made of Na metal anode and an air cathode where oxygen is taken from the environment while discharging. Based on the electrolytes, Na-air batteries are divided into two types; nonaqueous and aqueous.[151]

The charge-discharge mechanism for the electrolytic based hybrid Na-air battery can be explained by the following reactions:[152]

- *Anode:*

$$Na \rightarrow Na^{+} + e^{-} \qquad (2.71\ V) \qquad (1)$$

- *Cathode:*

$$O_2 + 4\ H^+ + 4e^- \rightarrow 2\ H_2O \qquad (1.23\ V) \qquad (2)$$

$$\text{Overall reaction:} \quad 4\ Na + O_2 + 4\ H^+ \rightarrow 2\ H_2O\ (3.94\ V)$$

The discharge products for Na–air batteries are diverse, where sodium superoxide (NaO_2) is the chief discharge product. The development of Na_2O_2, another discharge product, is thermodynamically preferred than NaO_2, but looking at the perspective from a kinetic point of view NaO_2 only needs a one-electron transfer that is comparatively easy to have. NaO_2 is reflected as an electronic conductor showing various properties for the charging process.[153]

The ORR and OER process in Na-air batteries face hinders from slow kinetics while undergoing discharge and charge process and produces a high overpotential gap.[154][155] A stable and active bifunctional electrocatalyst is highly demanded to promote the efficiency of hybrid Na−air battery and noble metal catalysts like Pt and Pt−based materials regarded as effective catalysts. However, higher cost, poor stability, and other factors made high demand to produce effective bifunctional electrocatalysts.[156][157] MOF and MOF derived materials extensively used owing to their superior surface area, hierarchical pores, and available functionalization for electrochemical catalysis of ORR and OER.

3.4.1. MOF-based Electrocatalysts for Na-air battery:

MOF−derived Co nanoparticles confined in N−doped carbon nanotubes were utilized in Na−air battery, which exhibited excellent electrochemical performance. The well-developed porous structure and the higher number of active sites along with the synergetic effect of the components, *i.e.*, N dopants and Co nanoparticles, made it perform efficiently in ORR and OER in Na-air batteries.[158] ZnCo bimetal organic framework (bi−MOF) was used to design exceptional extremely discrete Co nanoparticle decorated on N−doped defective carbon nano−framework (Co−N−C). Zinc evaporation results in a higher specific surface area that accelerates the adsorption and desorption of oxygen, leading to easy access catalytic sites. The ORR and OER can be processed with ease because of N−doped defective carbon and coexistence of CoN_x and Co set which perform as active sites. Interface electron transfer was facilitated by

the Co nanoparticles and carbon materials where rich Co−N−C species perform as durable bridging bonds. The large number of active sites, improved electrons transmission, and the synergetic coupled effect resulted in a low overpotential gap of 0.94 V between the OER potential and ORR. The half−wave potential exhibited excellent electrocatalytic performance. The Co−N−C−0.5 catalyst resulted in a low voltage gap of 0.31 V in Na−air battery where the round trip efficiency of 90.0% was attained at the current density of 0.1 mA/cm^2 along with an excellent cycle rate for charge and discharge.[159]

The hierarchical Co_3O_4@$MnCo_2O_{4.5}$ nanocubes having a hollow cage type assembly was prepared and utilized in Na–O_2 batteries as an effective air cathode catalyst. Three steps were used for synthesis, including templating with MOFs to assist synthetic route, surface etching, and high-temperature annealing. The yolk like structural design, superior surface area, a large number of active sites, and improved conductivity for electron diffusion in h-Co_3O_4@$MnCo_2O_{4.5}$ along with macropores and mesopores uniformly dispersed on the surface, provide effective O_2 diffusions pathways and enormously increase catalytic activity during the ORR and OER. The discharge product deposits on the surface of h-Co_3O_4@$MnCo_2O_{4.5}$ result in relatively loose morphology, which is favorable for the efficient reversibility of the Na–O_2 battery. Higher cyclic stability and efficiency enhancements in discharge–charge overpotential were achieved in Na-air batteries based on h-Co_3O_4@$MnCo_2O_{4.5}$.[160]

4. Conclusion

As energy continues to be one of the pivotal issues of the century, metal-air batteries are hereby discussed due to their solid position as a candidate for renewable energy storage, specifically solar energy, being the most attractive renewable energy source. The latest publications involving prominent synthesis methods and engineering strategies to fabricate outstandingly efficient MOFs were selected and elaborated in this review. This review endeavored to shed light on their vast potential as efficient functional materials for solar cells and metal-air batteries, combining most essential features; larger surface and area and highest conductivity. MOF derived carbon materials are also reported to provide a wide dispersion of versatile active sites ranging from metal, metal oxides, or non-metals, to further promote catalysis of oxygen reactions. This promising class of materials would successfully reduce the gap between energy-related discoveries made inside laboratories and the industrial sector.

The authors would like to express their deep accolade to the “State Key Laboratory of Advanced Technology for Materials Synthesis and Processing” for financial support.

6. References:

[1] M. T. Shaker, A. E. Khedr, S. Kholeif, *Journal of computer science* **2019**, *15*, 537.

[2] A. Kumari, S. Tanwar, S. Tyagi, N. Kumar, M. S. Obaidat, J. J. P. C. Rodrigues, *IEEE Wireless Communications* **2019**, *26*, 47.

[3] E. Apostolaki-Iosifidou, S. Woo, T. Lipman, *TRID* **2019**.

[4] IEA, *World Energy Outlook* **2019**.

[5] A. Gurung, Q. Qiao, *Joule* **2018**, *2*, 1.

[6] D. Tenfen, E. C. Finardi, B. Delinchant, F. Wurtz, *The institution of engineering and technology* **2016**, *10*, 576.

[7] Y. Li, J. Lu, *ACS energy letters* **2017**, *2*, 1370.

[8] Q. Li, Y. Liu, S. Guo, H. Zhou, *Nano today* **2017**, *16*, 46.

[9] E. Davari, D. G. Ivey, *Sustainable Energy & Fuels* **2017**, *2*, 39.

[10] C. D. Fiakas, *ALT enegy stocks* **2013**.

[11] A. Corma, H. Garcı, F. X. L. i Xamena, *Chemical Reviews* **2010**, *110*, 4606.

[12] A. I. Hönicke, I. Senkovska, V. Bon, I. Baburin, N. Boenisch, S. Raschke, J. D. Evans, *Angewandte Chemie - International Edition* **2018**, *57*, 13780.

[13] J. Lee, O. K. Farha, J. Roberts, K. A. Scheidt, S. T. Nguyen, J. T. Hupp, *Chem. Soc. Rev.* **2009**, *38*, 1450.

[14] W. L. Schram, I. Lampropoulos, W. G. J. H. M. Van Sark, *Applied Energy* **2018**, *223*, 69.

[15] E. D. Spoerke, L. J. Small, M. E. Foster, J. Wheeler, A. M. Ullman, V. Stavila, M. Rodriguez, M. D. Allendorf, *The Journal of Physical Chemistry C* **2017**, *121*, 4816.

[16] T. Chen, Y. Huang, C. Li, C. Kung, R. Vittal, K. Ho, *Nano Energy* **2016**, *32*, 19.

[17] A. S. A. Ahmed, W. Xiang, I. S. Amiinu, X. Zhao, *New Journal of Chemistry* **2018**, *42*, 17303.

[18] D. Shen, A. Pang, Y. Li, J. Dou, M. Wei, *Chemical Communications* **2018**, *54*, 1253.

[19] W. Xing, P. Ye, J. Lu, X. Wu, Y. Chen, T. Zhu, A. Peng, *Journal of Power Sources* **2018**, *401*, 13.

[20] B. O'Regan, M. Gratzel, *Letters to nature* **1991**, *353*, 737.

[21] A. Hagfeldt, G. Boschloo, L. Sun, L. Kloo, H. Pettersson, *Chemical Reviews* **2010**, *110*, 6595.

[22] K. Sharma, V. Sharma, S. S. Sharma, **2018**, *6*.

[23] M. Yeoh, K.-Y. Chan, *Energy Research* **2017**, *13*, 381.

[24] S. Aghazada, M. K. Nazeeruddin, *Inorganics* **2018**, *6*, 52.

[25] A. M. Ammar, H. S. H. Mohamed, M. M. K. Yousef, G. M. Abdel-hafez, A. S. Hassanien, A. S. G. Khalil, *Hindawi* **2019**, *2019*.

[26] H. Iftikhar, G. G. Sonai, S. G. Hashmi, A. Fl, P. D. Lund, *materials* **2019**, *12*, 1998.

[27] Y. He, Z. Zhang, W. Wang, L. Fu, *Journal of Alloys and Compounds* **2020**, *20*, 154089.

[28] Y. Li, A. Pang, C. Wang, M. Wei, *Journal of Materials Chemistry* **2011**, *21*, 17259.

[29] A. Gu, W. Xiang, T. Wang, S. Gu, X. Zhao, *Solar Energy* **2017**, *147*, 126.

[30] S. Alwin, V. Ramasubbu, X. S. Shajan, *Bulletin of Materials Science* **2018**, *41*, 27.

[31] W. A. Maza, A. J. Haring, S. R. Ahrenholtz, C. C. Epleya, S. Y. Lina, A. J. Morris, *Chemical science* **2015**, *7*, 719.

[32] J. Wu, Z. Lan, J. Lin, M. Huang, Y. Huang, L. Fan, G. Luo, Y. Lin, Y. Xie, Y. Wei, *Chemical Society Reviews* **2017**, *46*, 5975.

[33] Z. Jin, M. Zhang, M. Wang, C. Feng, Z. Wang, *Accounts of chelmical research* **2017**, *50*, 895.

[34] S. Gnanasekar, P. Kollu, S. K. Jeong, A. N. Grace, *Scientific Reports* **2019**, *9*, 5177.

[35] R. Kumar, V. Sahajwalla, P. Bhargava, *nanoscale advances* **2019**, *1*, 3192.

[36] G. Li, X. Gao, *Advanced Materials* **2019**, *1806478*, 1.

[37] J. Zhang, H. Zhou, D. Zhou, P. Liao, *National science review* **2018**, *5*, 907.

[38] A. H. He, Q. Sun, W. Gao, J. A. Perman, F. Sun, G. Zhu, B. Aguila, B. Space, S. Ma, *Angewandte Chemie - International Edition* **2018**, *57*, 4657.

[39] X. Ma, Y. Chai, P. Li, B. Wang, *Accounts of Chemical Research* **2019**, *52*, 1461.

[40] C. Chueh, C. Chen, Y. Su, H. Konnerth, Y. Gu, C. Kung, K. C. Wu, *Journal of Materials Chemistry A* **2019**, *7*, 17079.

[41] S. Liu, Z. Li, K. Zhao, M. Hao, Z. Zhang, L. Li, Y. Zhang, W. Zhang, *Journal of Alloys and Compounds* **2020**, *20*, 154910.

[42] J. Ou, J. Xiang, J. Liu, L. Sun, *ACS Applied Materials & Interfaces* **2019**, *11*, 14862.

[43] Y. Tian, Y. Wang, S. Chen, Z. Gu, J. Zhang, *ACS Applied Materials & Interfaces* **2019**, *12*, 1078.

[44] F. Bella, R. Bongiovanni, R. S. Kumar, M. A. Kulandainathan, A. M. Stephan, *Journal of Materials Chemistry A* **2013**, *1*, 9033.

[45] S. Sarwar, M. Lee, S. Park, T. T. Dao, A. Ullah, S. Hong, C. Han, *Thin Solid Films* **2020**, *20*, 30236.

[46] A. Kojima, K. Teshima, Y. Shirai, T. Miyasaka, *JACS* **2009**, *131*, 6050.

[47] N. transforming Energy, *NREL* **2019**.

[48] S. Seo, S. Jeong, H. Park, H. Shin, N.-G. Park, *Chemical communication* **2019**, *55*, 2403.

[49] X. Xu, J. Liu, J. Liu, L. Ouyang, R. Hu, H. Wang, L. Yang, M. Zhu, *Advanced Functional Materials* **2018**, *28*, 1707573.

[50] M. S. Javed, H. U. Shah, N. Shaheen, R. Lin, M. Qiu, J. Xie, J. Li, R. Raza, W. Mai, C. Hu, *Electrochimica Acta* **2018**, *18*, 31296.

[51] A. X. Hou, L. Pan, S. Huang, W. Ou-yang, X. Chen, *Electrochimica Acta* **2017**, *17*, 30701.

[52] M. L. Aubrey, B. M. Wiers, S. C. Andrews, T. Sakurai, S. E. Reyes-lillo, S. M. Hamed, C. Yu, L. E. Darago, J. A. Mason, J. Baeg, F. Grandjean, G. J. Long, S. Seki, *Nature Materials* **2018**, *17*, 625.

[53] A. V Vinogradov, H. Zaake-hertling, E. Hey-hawkins, A. V. Agafonov, G. A. Seisenbaeva, V. G. Kesslerd, V. V Vinogradov, *Chemical communication* **2014**, *1*, 14.

[54] C. Lee, C. Chen, Y. Liao, K. C. Wu, C. Chueh, *advanced science* **2018**, *6*, 1801715.

[55] U. Ryu, S. Jee, J. Park, I. K. Han, J. H. Lee, M. Park, K. M. Choi, *ACS Nano* **2018**, *12*, 4968.

[56] T. My, H. Nguyen, C. W. Bark, *ACS omega* **2020**, *5*, 2280.

[57] Y. Zhang, B. Li, L. Fu, Q. Li, L. Yin, *Electrochimica Acta* **2019**, *330*, 135280.

[58] M. Li, J. Wang, A. Jiang, D. Xia, X. Du, Y. Dong, P. Wang, R. Fan, Y. Yang, *Solar Energy* **2019**, *188*, 380.

[59] L. Huang, X. Zhou, R. Wu, C. Shi, R. Xue, J. Zou, C. Xu, J. Zhao, W. Zeng, *Journal of Power Sources* **2019**, *433*, 226699.

[60] X. Zhou, L. Qiu, R. Fan, A. Wang, H. Ye, C. Tian, S. Hao, Y. Yang, *RRL solar* **2019**, *4*, 1900380.

[61] T. Chang, C. Kung, H. Chen, T. Huang, S. Kao, H. Lu, M. Lee, K. M. Boopathi, C. Chu, *Advanced Materials* **2015**, *27*, 7229.

[62] X. Zhou, L. Qiu, R. Fan, J. Zhang, S. Hao, Y. Yang, *Nano-Micro Letters* **2020**, *12*, 80.

[63] O. A. Abdulrazzaq, V. Saini, S. Bourdo, E. Dervishi, A. S. Biris, *particulate science and technology* **2013**, *6351*, 427.

[64] L. Li, Z. Chang, X. Zhang, *advanced sustainable systems* **2017**, *1*, 1700036.

[65] J. Zhang, Q. Zhou, Y. Tang, L. Zhang, Y. Li, *Chemical science* **2019**, 8924.

[66] P. Nian, Y. Cao, Y. Li, X. Zhang, Y. Wang, H. Liu, X. Zhang, *CrystEngComm* **2018**, *20*, 2440.

[67] I. Imaz, M. Cano-sarabia, D. Maspoch, A. Carne, *nature chemistry* **2013**, *5*, 203.

[68] S.-Y. T, G.-M. M, M. R, M. A, G. R, H. P, S. C, C. P, *Angewandte Chemie - International Edition* **2017**, *56*, 15565.

[69] W. Liu, R. Yin, X. Xu, L. Zhang, W. Shi, X. Cao, *advanced science* **2019**, *6*, 1802373.

[70] H. Ji, M. Wang, S. Liu, H. Sun, J. Liu, T. Qian, C. Yan, *Electrochimica Acta* **2020**, *19*, 135562.

[71] G. Tian, M. Zhao, D. Yu, X. Kong, J. Huang, *Small* **2014**, *10*, 2251.

[72] Z. Song, X. Han, Y. Deng, N. Zhao, W. Hu, C. Zhong, *ACS Applied Materials & Interfaces* **2017**, *9*, 22694.

[73] B. Zhu, Z. Liang, D. Xia, R. Zou, *Energy Storage Materials* **2019**, *23*, 2405.

[74] EnergyTrend editor, *Trend force* **2017**.

[75] W. Tahil, *Meridian International Research* **2007**, 1.

[76] C. N. R. S. Upr, U. Pierre, P. Cedex, *Electrochemical society* **1992**, *139*, 644.

[77] X. Han, X. Ling, Y. Wang, T. Ma, C. Zhong, W. Hu, Y. Deng, *Angewandte Chemie* **2019**, *131*, 5413.

[78] Z. Liang, W. Guo, R. Zhao, T. Qiu, H. Tabassum, R. Zou, *Nano Energy* **2019**, *64*, 103917.

[79] G. Han, Y. Zheng, X. Zhang, Z. Wang, Y. Gong, C. Du, M. Norouzi, Y. Yiu, T. Sham, L. Gu, Y. Sun, Y. Wang, J. Wang, Y. Gao, G. Yin, X. Sun, *Nano Energy* **2019**, *66*, 104088.

[80] X. Zhang, X. Han, Z. Jiang, J. Xu, L. Chen, Y. Xue, A. Nie, Z. Xie, Q. Kuang, L. Zheng, *Nano Energy* **2020**, *71*, 104547.

[81] S. H. Lee, J. Kim, D. Y. Chung, J. M. Yoo, H. S. Lee, M. J. Kim, B. S. Mun, S. G. Kwon, Y. Sung, T. Hyeon, *Journal of the American Chemical Society* **2019**, *141*, 2035.

[82] X. Wang, Z. Chen, X. Zhao, T. Yao, W. Chen, R. You, C. Zhao, G. Wu, J. Wang, W. Huang, J. Yang, X. Hong, S. Wei, Y. Wu, Y. Li, *Angewandte Chemie - International Edition* **2017**, *57*, 1944.

[83] X. Hai, X. Zhao, N. Guo, C. Yao, C. Chen, W. Liu, H. Yan, J. Li, Z. Chen, X. Li, H. Xu, P. Lyu, *ACS Catalysis* **2020**, *10*, 5862.

[84] N. K. Wagh, S. S. Shinde, C. H. Lee, J. Jung, D. Kim, S. Kim, C. Lin, S. U. Lee, J. Lee, *Applied Catalysis B, Environmental* **2020**, *268*, 118746.

[85] Z. Wang, J. Ang, J. Liu, X. Yun, D. Ma, J. Kong, Y. Zhang, T. Yan, X. Lu, *Applied Catalysis B: Environmental* **2019**, *19*, 118344.

[86] S. Agarwal, X. Yu, A. Manthiram, *Materials Today Energy* **2020**, *16*, 100405.

[87] M. Wu, G. Zhang, J. Qiao, N. Chen, W. Chen, S. Sun, I. National, D. Recherche, S.-énergie Matériaux, *Nano Energy* **2019**, *61*, 86.

[88] J. Zhang, M. Zhang, Y. Zeng, J. Chen, L. Qiu, H. Zhou, C. Sun, *Small* **2019**, *1900307*, 1.

[89] D. Guo, R. Shibuya, C. Akiba, S. Saji, T. Kondo, J. Nakamura, *Science* **2016**, *351*, 361.

[90] S. Sarkar, A. Biswas, T. Purkait, M. Das, N. Kamboj, R. S. Dey, *Inorganic Chemistry* **2020**, *59*, 5194.

[91] T. Najam, S. Shoaib, A. Shah, H. Ali, Z. Song, H. Sun, Z. Peng, X. Cai, *Carbon* **2020**, *164*, 12.

[92] D. Wang, D. Su, *Energy & Environmental Science* **2014**, *7*, 576.

[93] I. O. Maciel, M. A. Pimenta, B. G. Sumpter, V. Meunier, F. Lo, *Nano Letters* **2008**, *9*, 2267.

[94] J. Zhang, L. Dai, *Angewandte Chemie - International Edition* **2016**, *55*, 1.

[95] B. He, F. Liu, S. Yan, *Journal of Materials Chemistry A* **2017**, *5*, 18064.

[96] J. Zhang, L. Dai, *ACS Catalysis* **2015**, *5*, 7244.

[97] Y. Xing, N. Chen, M. Luo, Y. Sun, Y. Yang, J. Qian, L. Li, *Energy Storage Materials* **2019**, *24*, 707.

[98] K. M. Abraham, Z. Jiang, *Journal of electrochemical society* **1996**, *143*, 1.

[99] F. Wu, Y. Yu, *Joule* **2018**, *2*, 815.

[100] Y. Wang, H. Zhou, *Journal of Power Sources journal* **2010**, *195*, 358.

[101] N. Lai, G. Cong, Z. Liang, Y. Lu, N. Lai, G. Cong, Z. Liang, Y. Lu, *Joule* **2018**, *2*, 1.

[102] Y. Wang, N. Lai, Y. Lu, Y. Zhou, C. Dong, Y. Lu, Y. Wang, N. Lai, Y. Lu, Y. Zhou, C. Dong, Y. Lu, *Joule* **2017**, *2*, 1.

[103] C. Jin, Z. Yang, X. Cao, F. Lu, R. Yang, *International Journal of Hydrogen Energy* **2013**, *39*, 2526.

[104] D. Geng, N. Ding, T. S. A. Hor, S. W. Chien, Z. Liu, *Advanced Energy Materials* **2016**, *6*, 1502164.

[105] Z. Lyu, G. J. H. Lim, R. Guo, Z. Kou, T. Wang, C. Guan, J. Ding, W. Chen, J. Wang, *Advanced Functional Materials* **2018**, *29*, 1806658.

[106] X. Meng, K. Liao, J. Dai, X. Zou, S. She, W. Zhou, F. Ye, Z. Shao, *ACS Applied Materials & Interfaces* **2019**, *11*, 20091.

[107] Y. Liu, H. Jiang, Y. Zhu, X. Yang, C. Li, *Journal Materials Chemistry A* **2016**, *4*, 1694.

[108] X. Wang, F. Zhang, Y. Liu, Z. Wang, *journal of the electrochemical society* **2018**, *165*, 3052.

[109] X. Wang, H. Zhang, H. Lin, S. Gupta, C. Wang, Z. Tao, H. Fu, T. Wang, J. Zheng, G. Wu, X. Li, **2016**, *25*, 110.

[110] M. Khalid, A. M. B. Honorato, L. Dai, *Nano Energy* **2017**, *17*, 30819.

[111] Y. Hou, C. Hou, Y. Zhai, H. Li, T. Chen, Y. Fan, H. Wang, W. Wang, *Electrochimica Acta* **2019**, *324*, 134884.

[112] F. Ma, H. Bin Wu, B. Y. Xia, C. Xu, X. Wen, D. Lou, *Angewandte Chemie* **2015**, *54*, 15395.

[113] Y. Jong, J. Hyun, S. Park, J. Park, J. Lee, Y. Chan, *Chemical Engineering Journal* **2018**, *351*, 886.

[114] T. G. Kelly, K. X. Lee, J. G. Chen, *Journal of Power Sources* **2014**, *271*, 76.

[115] Y. J. Oh, J. H. Kim, J. Y. Lee, S.-K. Park, Y. C. Kang, *Chemical Engineering Journal* **2019**, *19*, 32757.

[116] M. Zhang, Q. Dai, H. Zheng, M. Chen, L. Dai, *Advanced Materials* **2018**, *1705431*, 1.

[117] S. Li, Y. Dong, J. Zhou, Y. Liu, J. Wang, X. Gao, Y. Han, P. Qi, B. Wang, *Energy & Environmental Science* **2018**, *11*, 1318.

[118] F. Chao, B. Wang, J. Ren, Y. Lu, W. Zhang, X. Wang, L. Cheng, Y. Lou, J. Chen, *Journal of Energy Chemistry* **2019**, *35*, 212.

[119] J. Li, Y. Deng, L. Leng, M. Liu, L. Huang, X. Tian, H. Song, X. Lu, *Journal of Power Sources* **2020**, *450*, 227725.

[120] X. Hu, F. Cheng, N. Zhang, X. Han, J. Chen, *Small* **2015**, *2*, 5545.

[121] X. Zhang, P. Dong, J. Lee, T. Jake, Y. Cha, S. Ha, M. Song, *Energy Storage Materials* **2018**, *18*, 30801.

[122] H. Wang, F. Yin, N. Liu, R. Kou, X. He, C. Sun, B. Chen, D. Liu, H. Yin, *Advanced Functional Materials* **2019**, *29*, 1901531.

[123] A. Chatterjee, S. W. Or, *Electrochimica Acta* **2020**, *20*, 135809.

[124] R. Liang, A. Hu, M. Li, Z. Ran, C. Shu, J. Long, *Journal of Alloys and Compounds* **2019**, *810*, 151877.

[125] S. Yu, S. Luo, Y. Zhan, H. Huang, Q. Wang, *Journal of Power Sources* **2020**, *453*, 227899.

[126] Y. Zhao, Z. Song, X. Li, Q. Sun, N. Cheng, S. Lawes, X. Sun, *Energy Storage Materials* **2015**, *15*, 30056.

[127] D. R. Egan, C. P. De León, R. J. K. Wood, R. L. Jones, K. R. Stokes, F. C. Walsh, *Journal of Power Sources* **2013**, *236*, 293.

[128] Q. Li, N. J. Bjerrum, *Journal of Power Sources* **2002**, *110*, 1.

[129] C. Hang, J. Zhang, J. Zhu, W. Li, Z. Kou, Y. Huang, *Advanced Energy Materials* **2018**, *8*, 1703539.

[130] J. Xu, Z. Chang, Y. Wang, D. Liu, Y. Zhang, X. Zhang, *Advanced Materials* **2016**, *28*, 9620.

[131] R. Mori, *RSC Advances* **2017**, *7*, 6389.

[132] A. M. Abdel-Gaber, E. Khamis, S. Adeel, *Materials Chemistry and Physics* **2010**, *124*, 773.

[133] D. O. Flamini, S. B. Saidman, J. B. Bessone, *Corrosion science* **2006**, *48*, 1413.

[134] J. B. Bessone, D. O. Flamini, S. B. Saidman, *Corrosion science* **2005**, *47*, 95.

[135] Z. Zhang, C. Zuo, Z. Liu, Y. Yu, Y. Zuo, Y. Song, *Journal of Power Sources* **2014**, *251*, 470.

[136] M. Nestoridi, D. Pletcher, R. J. K. Wood, S. Wang, R. L. Jones, K. R. Stokes, I. Wilcock, *Journal of power sources* **2008**, *178*, 445.

[137] Y. Xu, Y. Zhao, J. Ren, Y. Zhang, H. Peng, *Angewandte Chemie* **2016**, *128*, 1.

[138] T. Zhang, Z. Li, Z. Zhang, L. Wang, P. Sun, S. Wang, *The Journal of Physical Chemistry C* **2018**, *48*, 27469.

[139] C. Wang, Z. Li, L. Wang, X. Lu, S. Wang, X. Niu, *Energy Technology* **2019**, *7*, 1900123.

[140] M. Jiang, J. Yang, J. Ju, W. Zhang, L. He, J. Zhang, C. Fu, B. Sun, *Energy Storage Materials* **2020**, *20*, 30022.

[141] Y. Liu, H. Jiang, J. Hao, Y. Liu, H. Shen, W. Li, J. Li, *ACS Applied Materials & Interfaces* **2017**, *9*, 31841.

[142] J. Li, N. Zhou, J. Song, L. Fu, J. Yan, Y. Tang, H. Wang, *acs sustainable chemistry and egineering* **2018**, *6*, 413.

[143] J. Wang, H. Lu, Q. Hong, Y. Cao, X. Li, J. Bai, *Chemical Engineering Journal* **2017**, *17*, 31415.

[144] P. Lou, C. Li, Z. Cui, X. Guo, *Journal of Materials Chemistry A* **2015**, *8*, 1703539.

[145] S. S. Zhang, D. Foster, J. Read, *Journal of power sources* **2010**, *195*, 1235.

[146] S. Wei, S. Xu, A. Agrawral, S. Choudhury, Y. Lu, Z. Tu, L. Ma, L. A. Archer, *Nature Communications* **2016**, *7*, 1.

[147] S. Choudhury, S. Wei, Y. Ozhabes, D. Gunceler, M. J. Zachman, Z. Tu, J. H. Shin, P. Nath, A.

Agrawal, L. F. Kourkoutis, T. A. Arias, L. A. Archer, *Nature Communications* **2017**, *8*, 898.

[148] X. Lu, G. Xia, J. P. Lemmon, Z. Yang, *Journal of Power Sources* **2010**, *195*, 2431.

[149] S. Kim, D. Seo, X. Ma, G. Ceder, K. Kang, *Advanced Energy Materials* **2012**, *2*, 710.

[150] M. Kim, H. Ju, J. Kim, *Journal of Materials Chemistry A* **2018**, *6*, 8523.

[151] E. Peled, D. Golodnitsky, H. Mazor, M. Goor, S. Avshalomov, *Journal of Power Sources* **2011**, *196*, 6835.

[152] Z. Khan, M. Vagin, X. Crispin, *advanced science* **2020**, *7*, 1902866.

[153] J. Kim, H. Lim, H. Gwon, K. Kang, *Physical chemistry chemical physics* **2013**, *15*, 3623.

[154] J. Suntivich, H. A. Gasteiger, N. Yabuuchi, H. Nakanishi, J. B. Goodenough, Y. Shao-horn, *Nature Chemistry* **2011**, *3*, 546.

[155] J. Suntivich, K. J. May, H. A. Gasteiger, J. B. Goodenough, Y. Shao-Horn, *Science* **2012**, *1383*, 1383−1385.

[156] J. Zhang, Z. Zhao, Z. Xia, L. Dai, *Nature Nanotechnology* **2015**, *10*, 444.

[157] Q. Chen, C. Hou, C. Wang, X. Yang, Y. Chen, *Chemical Communications* **2018**, *54*, 6400.

[158] Y. J. Wang, B. Fang, D. Zhang, A. Li, D. P. Wilkinson, A. Ignaszak, L. Zhang, *Electrochemical Energy Reviews* **2018**, *1*, 1.

[159] J. Zhu, T. Qu, F. Su, Y. Wu, Y. Kang, K. Chen, Y. Yao, W. Ma, B. Yang, Y. Dai, F. Liang, D. Xue, *Dalton Transactions* **2020**, *49*, 1811.

[160] Y. Liu, L. Xiaowei, C. Qi, H. Yuexiu, D. Jiaqi, H. Xinghao, L. Yu, *Nanoscale* **2019**, *11*, 5285.